TÉCNICO LISBOA

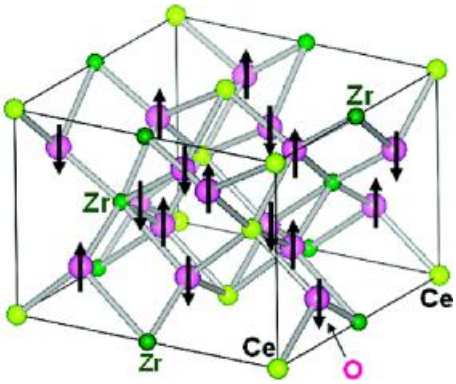

Production of a catalyst in supercritical fluid

Pure and doped ceria support catalyst

Raquel Filipa Magalhães Gomes

Thesis to obtain the Master of Science Degree in

Chemical Engineering

Supervisors: Dr. Cyril Aymonier (ICMCB)
Professor Carlos Manuel Faria de Barros Henriques (IST)

Examination Committee

Chairperson:	Professor Sebastião Alves
Supervisor:	Professor Carlos Manuel Faria de Barros Henriques
Vogal:	Professor José Madeira Lopes

December 2016

Acknowledgements

I would like to thank Dr. Cyril Aymonier for the possibility to work at *ICMCB* under his guidance and welcoming for the duration of the thesis and to Prof. Carlos Henriques to open the door that made this opportunity possible.

I would like to thank everybody from Group 7, especially Aimery and Cédric for all the time that you took to explain and teach what I needed to know.
I am also grateful for the people from *ICMCB* that made possible all the analysis that I needed done.

To the people I met while in Bordeaux, Jana, Beste and Esra, and to the friends from Portugal in Bordeaux, Margarida and Mariana, thank you for the company and for the fun.

I would like to thank all my friends for their support and friendship, especially to Mónica which although in Portugal put up with me.

Finally, I would like to thank my family without you nothing of this would have been possible, mostly to my mother for always been there for me and for picking me up when I needed.

Abstract

The present thesis had as objective to synthesize and characterize a catalyst support with particles with nanometric dimensions, namely a ceria-zirconia oxide catalyst support.

The catalyst support was produced under supercritical conditions and characterized with X-Ray Diffraction, Transmission Electron Microscopy, Inductively Coupled Plasma and BET analysis.

Different parameters were studied as the effect of the solvent, the effect of the quantity of cerium in the catalyst support and finally the effect of the residence time of the synthesis. For the analysis of the effect of solvent, two solvents were used namely distilled water and propanol. For the case of the study of the effect of the quantity of cerium, there was the substitution of cerium with zirconium ($Ce_{1-x}Zr_xO_2$ - x=0; 0,25; 0,50; 0,75;1) using distilled water as solvent. The residence times used in this study were 10s, 30s and 60s.

From these characterizations, it was possible to conclude that when propanol is the solvent the particles are smaller and that with the increase of residence time there is an increase of the crystallite size. It is also worth to note that the particles are single crystals.

As for the study of the composition of the catalyst support, a small effect of the Zr content was observed in the particle size of the catalyst support. In relation to the specific surface area, the produced catalyst support presented a range of values from 130 m^2/g to 230 m^2/g, with an increase of this value with a decrease of cerium percentage.

Keywords: ceria; ceria-zirconia; catalyst; support; supercritical; solvothermal; synthesis

Resumo

O objectivo da presente tese teve por base a síntese e caracterização de um catalisador constituído por partículas com dimensões nanométricas, nomeadamente um catalisador de óxido de cério-zircónio.

Para a realização destes objectivos, foi concebido um catalisador preparado em condições supercríticas, tendo-se pprocedido à sua caracterização através das seguintes técnicas: Difracção Raios-X, Microscópio Electrónico de Transmissão, análise BET e Espectrometria de Emissão com Plasma Indutivo.

A síntese do catalisador foi realizada com vários parâmetros, nomeadamente diversos solventes, diferentes quantidades de cério no catalisador e diferentes tempos de residência. No caso dos solventes, foi usado água destilada e propanol. No estudo das diferentes composições de cério foi também utilizada água destilada como solvente e as composições utilizadas foram 100%, 75%, 50%, 25% e 0% de cério. Para os tempos de residência recorreu-se a tempos de 10s, 30s e 60s.

A partir destas caracterizações foi possível concluir que os diferentes solventes resultam em tamanhos de partículas distintos, nomeadamente que o uso do propanol dá origem a partículas de tamanho menor. Também se observou que quanto maior é o tempo de residência, maior é o tamanho do cristal.

Em relação ao estudo da composição do catalisador, observa-se que o catalisador é composto por partículas monocristais e que a quantidade de cério na amostra não provoca alterações relevantes no tamanho das mesmas. As áreas superficiais alcançadas variam entre 130 m^2/g e 230 m^2/g, ou seja, há um aumento desta característica com a diminuição da percentagem de cério.

Palavras-chave: cério; cério-zircónio; supercrítico; catalisador; solvotérmico; síntese

Contents

List of Figures

List of Tables

Nomenclature

ΔG_v	Gibbs free energy per unit of volume ($\mathrm{J\ m^{-3}}$)
$\Delta\mu$	Chemical potential of system (J)
γ	Activity coefficient
λ	X-ray wavelength (nm)
μ	Viscosity ($\mathrm{Pa\ s^{-1}}$)
Ω	Atomic volume ($\mathrm{m^3}$)
ω	Constant determined by reaction system ($\mathrm{kg\ m^{-1}\ s^{-3}}$)
ρ_i	Density at inlet of reactor($\mathrm{kg\ m^{-3}}$)
ρ_r	Density in reactor ($\mathrm{kg\ m^{-3}}$)
θ	Position (°)
ε	Dielectric constant
a	Lattice parameter (Å)
AES	Atomic Emission Spectroscopy
B	BET constant
BET	Brunauer–Emmett–Teller
C	Solute concentration ($\mathrm{mol\ m^{-3}}$)
C_0	Equilibrium concentration or saturation ($\mathrm{mol\ m^{-3}}$)
d_{cr}	Crystallite diameter (nm)
$FWHM$	Full Width at Half Maximum (°)
HP	High pressure
HPP	High pressure pump
ICP	Inductively Coupled Plasma
k	Reaction rate ($\mathrm{mol\ m^{-3}\ s^{-1}}$)
k_0	Reaction rate correspondent to dielectric constant ε_0 ($\mathrm{mol\ m^{-3}\ s^{-1}}$)
k_B	Boltzmann constant ($\mathrm{m^2\ kg\ s^{-2}\ K^{-1}}$)
M	Molecular weight ($\mathrm{kg\ mol^{-1}}$)

m	Mass of the solid sample or adsorbent (g)
N	Avogadro's Number (mol^{-1})
NP	Nanoparticles
OSC	Oxygen Storage Capacity
P	Pressure (MPa)
P/P_0	Relative pressure
P_{amb}	Room pressure (MPa)
P_c	Critical Pressure (MPa)
P_r	Pressure in reactor (MPa)
Pr	Propanol
$PrOH$	Propanol
PSA	Pressure Swing Absorber
Q	Flow rate ($\mathrm{L\ min}^{-1}$)
R	Ideal gas constant ($\mathrm{J\ K}^{-1}\ \mathrm{mol}^{-1}$)
$RWGS$	Reverse Water Gas Shift
s	Adsorption cross section of the adsorbing species (m^2)
S_{BET}	Specific surface area ($\mathrm{m}^2\ \mathrm{g}^{-1}$)
s_s	Supersaturation
S_{Total}	Total surface area (m^2)
sc	Supercritical
SCF	Supercritical Fluid
SCW	Supercritical water
SMR	Steam methane reforming
T	Temperature (K or ℃)
T_{amb}	Room temperature (℃)
T_b	Boiling Temperature (℃)
T_c	Critical Temperature (℃)
T_r	Temperature in reactor (℃)
t_r	Residence time (s)
TEM	Transmission Electron Microscopy
TPR	Temperature Reduction Program
V_r	Reactor volume (dm^3)
W	Water

W	Weight of gas adsorbed (kg)
W_m	Weight of adsorbate as monolayer (kg)
WGS	Water Gas Shift
x	Percentage of Zirconium in $Ce_{1-x}Zr_xO_2$
XRD	X-Ray Diffraction

Chapter 1

Introduction

1.1 Motivation

This thesis integrates the project NiCe (international project between France-Poland-Russia) that has as objective to produce a Ni supported Ceria-Zirconia catalyst, to be used for the production of hydrogen. More specifically, the thesis is focused on ceria based monocrystals together with the impact of cerium substitution with zirconium ($Ce_{1-x}Zr_xO_2 - 0 \leq x \leq 1$).

The production of hydrogen has been growing and one of the reasons is the fact that hydrogen has a key role in the future production of sustainable energy. Namely, by using fuel cells which eliminate emissions and have higher efficiency than internal combustion engines in converting chemical energy of the fuel into electrical energy. However, hydrogen production remains a challenge since the biggest source also results from fossil fuels. The most used method for its production is the steam methane reforming (SMR), that uses methane ($\mathrm{CH_4}$) as raw material which the source is natural gas.

In order to accelerate the process and to obtain acceptable reaction rates, it is necessary to use a catalyst, which consequently will minimize the impact of using natural gas. This catalyst to be suitable for the production of hydrogen has to be stable under extreme conditions, as per example high temperatures (700℃ to 1100℃). Also, CeO_2 is refractory which means it needs high temperatures to be produced. So, a process using supercritical fluids enables a fast and simple step synthesis at moderate temperature due the specific properties of this fluids. This happens because of the low dielectric constant and solubility in the solvent that enhances a high supersaturation degree. It is also a process without many treatments, such as calcination, reduction, phase separation, etc., after the catalyst production .

Nowadays, in industry, it is already used in steam reforming a nickel supported by ceria catalyst. The use of nickel is due to the fact that it is relatively cheap and accessible when comparable with noble metals. In this thesis, it was decided to study the effect in the characteristics of the support using a combination of ceria and zirconia instead of just ceria. The catalyst support will be produced under supercritical conditions, which is considered the implementation of green chemistry. This is a subject that has been growing and becoming more relevant. Following, there is a small explication of this concept and why it is applicable to supercritical fluids (SCF).

1.1.1 Green Chemistry

The chemical industry has been having a shift in the mindset where more environmentally acceptable processes are growing in need. This shift is due to a bigger focus on environmental responsibility, which means eliminate waste at the source and avoid use of toxic and/or hazardous substances could bring economic value to the industry.
The book "Green Chemistry Using Liquid and Supercritical Carbon Dioxide" [1] defines Green Chemistry as *carrying out chemical activities - including chemical design, manufacture, use and disposal - such that hazardous substances will not be used and generated*. So, it is the design of an environmentally benign product and process. One of its objectives is to eliminate waste at source, preventing its formation instead of waste remediation and also reduce environmental impacts and energy usage. [2]

The use of SCF can be considered green chemistry due to the increase of the reaction rate or the fact that the solubility increases with the application of a solvent in supercritical state. Still, because of the operating conditions (high temperature and high pressure) of the processes in supercritical state, the energy requirements surpass the benefits above mentioned. So, the reason SCF are considered green is the fact they replace the organic solvents with a more harmless SCF, usually water or carbon dioxide. [3, 4]

1.2 Objectives

The objective of this thesis is to produce a $\mathrm{Ce_{1-x}Zr_xO_2}$ catalyst support for different values of x (0; 0,25; 0,5; 0,75 and 1). The production will be done in supercritical conditions and different parameters of production will be applied, such as residence time in the reactor and solvents. The solvents used are distilled water and propanol and the residences time implemented are 10s, 30s, and 60s.
Then, the catalysts support produced will be characterized through characterization techniques such as X-Ray Diffraction (XRD), BET analysis, Transmission Electron Microscopy (TEM) and Inductively coupled plasma atomic emission spectroscopy (ICP-AES). With the XRD characterization will be possible to observe the XRD pattern, calculate the crystallite size and the lattice parameter. The BET analysis will allow to know the specific surface area of the catalyst support. By using TEM, we will obtain an image of the particles of the catalyst support, being consequently possible to get by measure the average particle size. The ICP technique will provide the concentration of cerium in the catalyst support, in order to compare with the expected value.

After the characterization, the samples will go to the next phase of the project where they will be subjected to impregnation with nickel nanoparticles.

1.3 Thesis Outline

After the Chapter 1, the thesis includes a chapter called 'Literature Review' (Chapter 2) where there is information about the production of hydrogen and catalysts, supercritical fluids and characterization techniques. In Chapter 3 ('Methodology'), it is possible to read about the methodology which includes the chemicals used, operating conditions, apparatus and how to prepare the samples for each characterization technique.
In Chapter 4 ('Results and Discussion'), it will explain the results obtained from the characterization and

a discussion about them. Lastly, the thesis finishes with a chapter designated 'Conclusion and Future Work' that resumes everything and explains the results obtained and some possible future works.

Chapter 2

Literature Review

In this section, a general approach about the different ways to produce hydrogen, what it is a supercritical fluid and the process to produce the catalyst using this fluid will be done. There will be also an explanation of why this catalyst was chosen. At the end of this chapter, there is a small section about how the most important characterization techniques for this catalyst support works.

2.1 Production of hydrogen

There are two big different ways to produce hydrogen: steam reforming and partial oxidation. In the first method, the reactant is subject to steam, at high temperatures and pressure, and in the presence of a catalyst, producing hydrogen, carbon monoxide and a small quantity of carbon dioxide. In the second method, the reagent reacts with a limited amount of oxygen, not enough to completely oxidize the reagent to carbon dioxide and water, and it will produce the same products as the steam reforming. Another difference between the methods is that the first one is an endothermic process, so it's necessary to supply heat, oppositely, the second one is exothermic, thus giving heat. So, while steam reforming is favoured by high temperatures, and low pressures due to volume expansion, partial oxidation is favoured by low temperatures and pressure is not important.
In both cases, the reactions are accompanied by a water-gas shift (WGS) reaction (Eq. (2.1)) and a pressure-swing adsorption. The last one is used to remove carbon dioxide and impurities from the gas stream, what leaves pure hydrogen essentially. An interesting feature of WGS reaction is that it consumes the carbon monoxide produced to form more hydrogen [5, 6, 7, 8, 9, 10, 11].

$$\mathrm{CO} + \mathrm{H_2O} \longrightarrow \mathrm{CO_2} + \mathrm{H_2} \tag{2.1}$$

It is possible to increase the conversion in steam reforming by increasing the quantity of steam [12] because it increases the extent of steam reforming and WGS reactions, reducing the amount of unwanted products (CO and $\mathrm{CH_4}$). Although, it has as consequence a larger consumption of energy to produce steam necessary.

If both methods (exothermic partial oxidation and endothermic steam reforming) are combined, an adiabatic reaction occurs known as oxidative steam reforming or auto-thermal reforming. Instead of excess of steam to increase conversion, it is introduced oxygen that it will improve the conversion without decreasing the catalytic activity [5, 6, 13, 14, 10, 11].

The reagent for the production of hydrogen can be methane or other hydrocarbons (Table 2.1), alcohols (Table 2.2), such as ethanol and methanol, propane, gasoline, carbon dioxide, etc.

The various processes of production generate different H_2/CO ratios, where steam reforming produces the higher ratio while the partial oxidation the lowest. The oxidative steam reforming is in between but it has an acceptable value.

Table 2.1: Chemical reactions for different methods to produce hydrogen using hydrocarbons.

Method	Chemical reaction	
Steam reforming	$C_nH_{2n+2} + nH_2O \longrightarrow nCO + (2n+1)H_2$	(2.2)
Partial oxidation	$C_nH_{2n+2} + \left(\frac{n}{2}\right)O_2 \longrightarrow nCO + (n+1)H_2$	(2.3)
Oxidative steam reforming	$C_nH_{2n+2} + \left(\frac{n}{2}\right)H_2O + \left(\frac{n}{4}\right)O_2 \longrightarrow nCO + \left(\frac{3n+2}{2}\right)H_2$	(2.4)

Table 2.2: Chemical reactions for different methods to produce hydrogen using alcohols.

Method	Chemical reaction	
Steam reforming	$C_nH_{2n+1}OH + (n-1)H_2O \longrightarrow nCO + 2nH_2$	(2.5)
Partial oxidation	$C_nH_{2n+1}OH + \left(\frac{n-1}{2}\right)O_2 \longrightarrow nCO + (n+1)H_2$	(2.6)
Oxidative steam reforming	$C_nH_{2n+1}OH + \left(\frac{n-1}{2}\right)H_2O + \left(\frac{n-1}{4}\right)O_2 \longrightarrow nCO + \left(\frac{3n+1}{2}\right)H_2$	(2.7)

When methanol ($n = 1$) is used as a reagent, the equations in Table 2.2 do not apply. Instead, the equations that can be applied can be seen in Table 2.3.

Table 2.3: Chemical reactions for different methods to produce hydrogen using methanol.

Method	Chemical reaction	
Steam reforming	$CH_3OH + H_2O \longrightarrow CO_2 + 3H_2$	(2.8)
Partial oxidation	$CH_3OH + \left(\frac{1}{2}\right)O_2 \longrightarrow CO_2 + 2H_2$	(2.9)
Oxidative steam reforming	$CH_3OH + \left(\frac{3}{4}\right)H_2O + \left(\frac{1}{4}\right)O_2 \longrightarrow CO_2 + \left(\frac{11}{4}\right)H_2$	(2.10)

The use of alcohols instead of hydrocarbons is advantageous because in the presence of water, they disintegrate easily, generating a mixture rich in hydrogen at relatively low temperatures. However, it is also important to mention that methanol is highly toxic and it comes from non-renewable sources. In other hand, ethanol is less toxic and can be produced by fermentation of renewable resources (e.g. biomass). [12, 15, 16]

As it was mentioned in Section 1.1 steam reforming of methane is the major industrial hydrogen source but has the disadvantage to use fossil fuels, namely natural gas. This process of production is constituted of three main components:

- Furnace: where gas and steam travel down into reformer tubes in vertical rows which are surrounded by gas burners that heat the mix. The tubes are full of catalyst (nickel based catalyst).
- Water-gas shift reactor: this reactor is also filled with catalyst (iron-chrome based catalyst) and causes steam to break into oxygen and hydrogen. The last one goes for the rest of the process while the oxygen joins the carbon monoxide from the furnace and produces carbon dioxide.

- Pressure swing absorbers (PSAs): filters the remaining traces of CO, $\mathrm{CO_2}$, steam, $\mathrm{CH_4}$ from the $\mathrm{H_2}$. The impurities are then used as fuel for the furnace.

Other way to produce hydrogen is by using carbon dioxide and methane (Eq. (2.11)), also known as dry-reforming, that has the advantage of using greenhouse gases and turning them into valuable products. Nevertheless, it also happens reverse water-gas shift (RWGS) (Eq. (2.12)), that uses the hydrogen produced to form water. [8, 17, 18, 19]

$$\mathrm{CO_2 + CH_4 \longrightarrow 2CO + 2H_2} \tag{2.11}$$

$$\mathrm{CO_2 + H_2 \longrightarrow CO + H_2O} \tag{2.12}$$

Another problem with this technique is that at pressures just above 5 atm, the RWGS reaction begins to dominate the dry-reforming reaction. This occurs due to the preference for carbon dioxide to react by Equation (2.12) than by Equation (2.11), because hydrogen is more reactive than methane.
There is not yet industrial technology for $\mathrm{CO_2}$ reforming and it has high energy costs.
Summing up, there is two big ways to produce hydrogen: steam reforming and partial oxidation. The reagent for both can be hydrocarbons, alcohols, gasoline, etc. Besides of the reaction for the production of hydrogen, it also happens a water-gas shift reaction that produces more hydrogen and consumes carbon dioxide.
In the next section, it is possible to read about the production of catalyst used in this reactions, namely the solvothermal synthesis technique using supercritical fluids.

2.2 Production of catalysts support

2.2.1 Characteristics of catalyst

The catalyst for the hydrogen production has to have as main characteristics [34]:

- Catalyse the desirable reactions such as hydrogen abstraction from the fuel molecules to initiate reaction
- Promote water-gas shift reaction to minimize the CO conversion to methane via methanation reactions
- Be unfavourable for the undesired reactions such as methanation reactions

So, it is necessary a catalyst that as a high stability, activity, and selectivity towards hydrogen, supports severe conditions and consequently help employ smaller equipment. The utilization of a catalyst is to obtain satisfactory reaction rates in order to accelerate the process. This catalyst is expected to be a nanomaterial, which are identified by their unique properties, such as chemical, mechanical and thermal properties. A nanomaterial is a structure that has at least one of its phases in the nanometer size range. [21]

The catalyst chosen to proceed for the production of hydrogen was nickel supported by cerium-zirconium oxide ($\mathrm{Ni/Ce-ZrO_2}$). Nickel has been most widely used due to it is low cost compared with noble gases and availability but yet it is less active and normally more prone to deactivation. [35, 14, 18, 21, 8, 36]

The employment of a support is important because it decides the dispersion of the catalytically active metal particles or the resistance to sintering of the catalyst, affects the reactivity and coke resistance of

the metal particles and may participate in the catalytic reaction itself. The support also has the purpose of helping provide a stable and high active surface area. Thus, a strong interaction between metal and support makes a catalyst more resistant to sintering and coke formation, consequently its stability will last longer. Supports also avoid the agglomeration and the oxidation of nanoparticles, conserving the intrinsic properties and morphologies. [34, 21, 35, 37, 38, 39]
Given this, it is decided to add a support to nickel. The support chosen is ceria-zirconia which makes the catalyst acquire the capacity to store, release and transfer oxygen, therefore increasing the ability to prevent carbon formation.

When zirconia is introduced with ceria, it is a way to control the properties of the catalyst support using a technique known as doping, which basically is the incorporation of ions in the crystal lattice of the CeO_2. It is also used to increase the mobility of oxygen, increasing the catalytic properties. [32]

Some of the characteristics of ceria-zirconia support are the high oxygen storage capacity (OSC), the strong interaction between nickel and $\mathrm{CeZrO_2}$, thermal stability, high surface area and high capability of $\mathrm{H_2}$ uptake. Also, cerium-zirconium mixed oxides promote the water-gas shift reaction and the redox properties of many catalysts for the oxidation of hydrocarbons. It is important to accentuate that the support influences the catalyst activity by altering the electron donating ability of the reduced nickel surfaces. [9, 10, 14, 39, 40, 41, 42, 43]

The combination ceria-zirconia has other proposes besides being catalyst support for hydrogen production, it is also applied for glass polishing, ultraviolet absorbers, ceramics, etc. [39]

Catalysts with higher metal dispersion, smaller active site particles and larger OSC give a higher catalytic activity. Also, higher active surface area of the catalyst means a greater number of product molecules produced per unit of time, this is related to the activity of the catalyst. Another relevant factor for catalytic activity is the dispersion of particle, this is the ratio between the number of surface atoms and the total number of atoms. So, a higher dispersion normally represents smaller particle size, which improves the activity of the catalyst. Also, normally, ultrafine particles have very high specific surface area due to their small sizes which is a good characteristic because catalytic reactions take place at the surface. [43]

To resume, ceria-zirconia support help promote the reactions for producing hydrogen and its most important characteristics are the high storage capacity, thermal stability and high surface area. The following subsection introduces the method for its production.

2.2.2 Technique of production

There are a lot of techniques to produce nanoparticles (NP). Some of them are the following: physical vapour deposition, sol-gel, solvothermal/hydrothermal synthesis, co-precipitation, electrodeposition, impregnation, etc. Except for solvothermal synthesis, these methods are time and energy consuming, environmentally unfriendly and when nanoparticles are wanted, their complexity increases. [44, 35, 39, 45, 46, 47]

In nanotechnology, hydrothermal synthesis has a lead over the other techniques. This method is simple, cost effective, energy saving, pollution-free, has a better nucleation control, higher dispersion and rate of reaction and better shape of control. Other advantages are that accelerates interactions between solid and fluid species, can achieve pure phases and homogeneous materials. The solvothermal fluids offer higher diffusivity, low viscosity, facilitate mass transport and higher dissolving power. [44, 48] In Table 2.4, there is a small differentiation between three different techniques used in solvothermal synthesis.

Table 2.4: Different terminologies used in the solvothermal technique. [32]

	Temperature	Pressure
Conventional solvothermal	Above boiling point of the solvent and below its critical temperature ($T_b < T < T_c$)	Below critical pressure of solvent ($P < P_c$)
Solvothermal in subcritical medium	Below critical temperature ($T_b < T < T_c$)	Above critical pressure ($P > P_c$)
Solvothermal in supercritical medium	Above critical temperature ($T > T_c$)	Above critical pressure ($P > P_c$)

For the synthesis of NP, the high dissolving power is not a good characteristic. It is preferred to have a low solubility so that it is possible to obtain higher supersaturation degrees and suppress crystal growth. [44] Supersaturation can be considered the driving force for crystal nucleation and growth, where nucleation is the formation of new crystal nuclei. Crystal growth and supersaturation are normally competing mechanisms and determine the final crystal size distribution. In one hand, if supersaturation is low than crystals grow faster than they nucleate resulting in a larger crystal size. In the other hand, if supersaturation is higher, crystal growth is dominated by crystal nucleation and consequently smaller crystals are formed. In Figure 2.1, a graph relating supersaturation with different factors such as crystal size, nucleation rate and growth rate can be consulted. [49, 50]

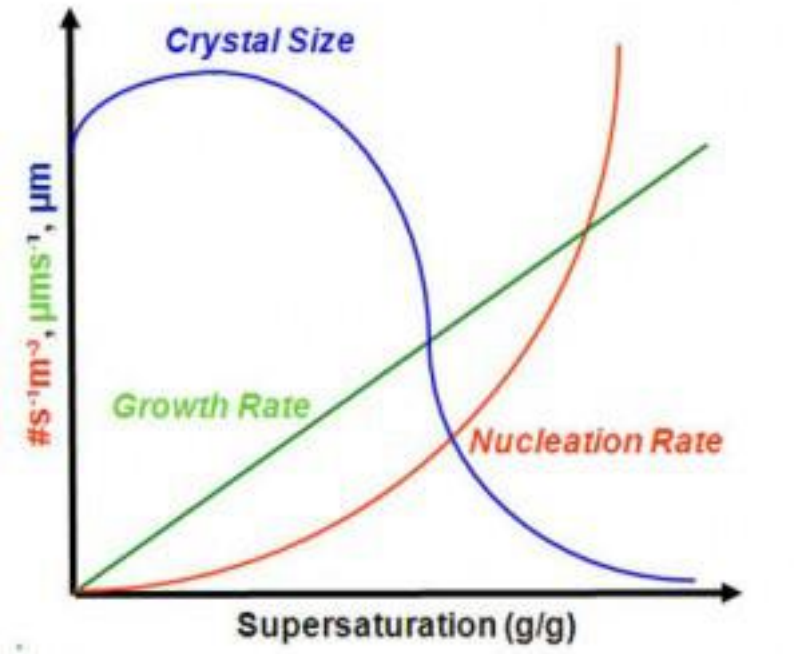

Figure 2.1: Relation between supersaturation and crystal size, nucleation rate and growth rate. [50]

The next part it will give a explanation about supercritical fluids, being this medium where the synthesis occurs and also helping understand why the medium was chosen.

2.2.2.1 Supercritical Fluids

Supercritical state is defined as the domain at which the distinction between the liquid state and the gaseous state disappears and the material exists as a fluid (Fig. 2.2 and Fig. 2.3) [20]. This is obtained when the critical point is reached, which has as coordinates the critical temperature ($\mathrm{T_c}$) and the critical pressure ($\mathrm{P_c}$). [21, 22, 23] In Figure 2.2, the solid lines represent the equilibrium between two phases and at the triple point the 3 phases coexist. Moreover, as the gas-liquid curve is ascended, the liquid becomes less dense due to thermal expansion and the gas more dense as the pressure increases. When these densities match, it means that the distinction between liquid and gas disappears, reaching the critical point. [24] Also, in this Figure 2.2, it is possible to observe the feasibility of going from a liquid phase to a gas phase without boiling the solution, instead going through the supercritical region. In this region, properties, such as density, viscosity, diffusion coefficient and thermal conductivity, change. A fluid in supercritical conditions has some of the advantageous properties of both liquid and gas phases, also it does not have surface tension neither enthalpy of vaporization. [22, 25, 26] In Table 2.5, a comparison of some properties between gases, liquids and supercritical fluids can be seen.

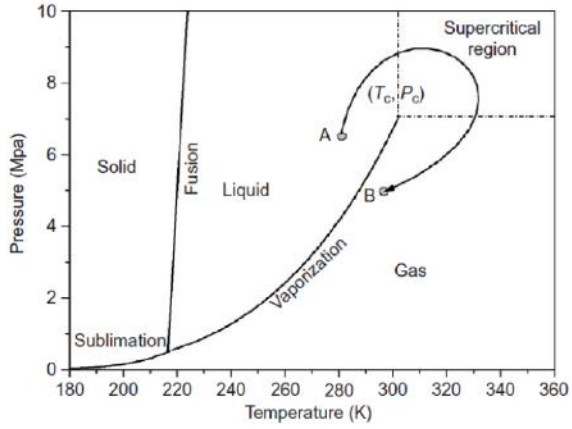

Figure 2.2: Temperature-pressure diagram of pure substance. [21]

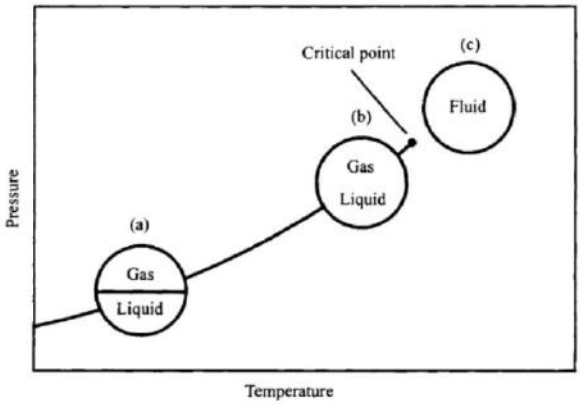

Figure 2.3: Meniscu evolution diagram. [24]

Table 2.5: Comparison of properties of gases, SFCs and liquids. [27]

	Density (kg/m^3)	Viscosity ($\mu Pa.s$)	Diffusivity (mm^2/s)
Gases	1	10	1 - 10
SCFs	100 - 1000	50 - 100	0,01 - 0,1
Liquids	1000	500 - 1000	0,001

Some advantages of using supercritical fluids (SCFs) are high diffusion rates, low viscosity, adjustable density, high miscibility with gases and high diffusion rates. [25, 22] One of the reasons that SCFs are starting to have more success in industry, it is due to the fact that the properties of the reaction medium are able to be adjusted at will with slightly variations in pressure and/or temperature. [20, 21, 25]

At temperatures not too far below $\mathrm{T_c}$ the liquid phase is called 'subcritical liquid', while for 'subcritical gases' is when the pressure is below $\mathrm{P_c}$. [22]

At supercritical conditions, the dielectric constant and the density of solvents varies greatly and

as consequence the solubility of metal oxides. This solubility decreases as the reaction temperature increases at a set pressure, resulting in the formation of nanoparticles. The variation of the dielectric constant and of the density with the temperature can be seen for water in Fig. 2.4 and Fig. 2.5, respectively. When the dielectric constant is high, the chemical potential of ions to lowers and the stabilization of ions induces the dissociation of electrolytes. [28, 29, 20, 30]

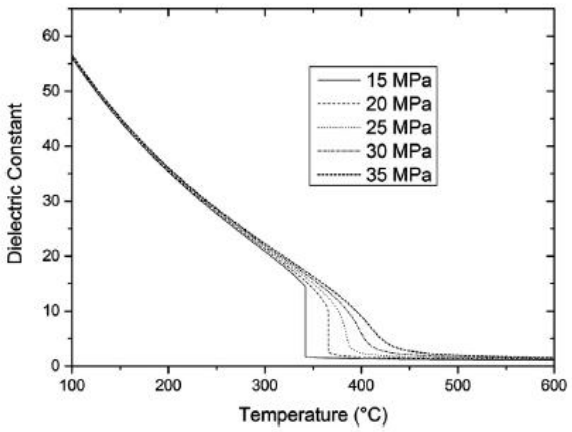

Figure 2.4: Dielectric constant of water at various temperatures and pressures. [31]

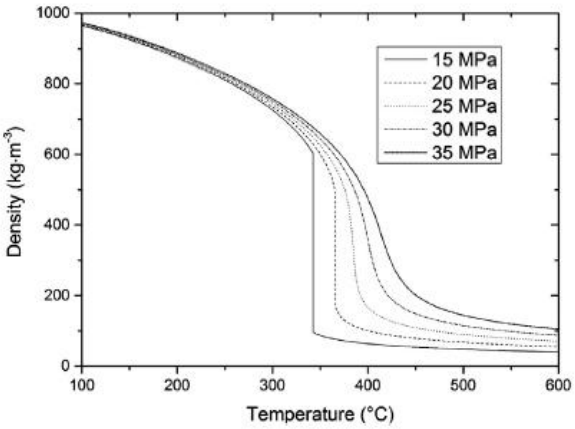

Figure 2.5: Density of water at various temperatures and pressures. [31]

According to the Nucleation Theory, its rate depends of the degree of supersaturation and the surface energy, so if there is a decrease in solubility is expected a higher degree of supersaturation. Under supercritical conditions is anticipated an extremely high nucleation and consequently the formation of nanoparticles of metal oxides. Also, the supercritical domain produces lower solubility favouring the nucleation by precipitation. [20, 23]

The growth of particles is associated with Gibbs Free Energy, because reducing this energy helps the nucleation process and consequently the particles grow. So, when the solute concentration, C, surpasses the equilibrium concentration or saturation, C_0, the total energy is reduced by the segregation of the solute in the solution.

It is possible to determine the Gibbs free energy per unit of volume, ΔG_v, which depends on the solute concentration, using Equation (2.13), where k_B is the Boltzmann constant, T is the absolute temperature and Ω is the atomic volume.

$$\Delta G_v = -\frac{k_B T}{\Omega} \ln\left(\frac{C}{C_0}\right) \tag{2.13}$$

The value of supersaturation (s_s) can also be calculate resorting to Equation (2.14), where $\Delta\mu$ is the chemical potential of the system and γ and γ_0 are the activity coefficients.

$$s_s = \frac{\Delta\mu}{k_B T} = \ln\left(\frac{\gamma.C}{\gamma_0.C_0}\right) \tag{2.14}$$

However, the activity coefficients can be neglected for low concentrations, which means $\gamma/\gamma_0 = 1$.

$$s_s = \ln\left(\frac{C}{C_0}\right) \tag{2.15}$$

Consequently, Equation (2.13) can be adjust and it is now represented by Equation (2.16).

$$\Delta G_v = -\frac{k_B T}{\Omega} s_s \tag{2.16}$$

Nucleation happens naturally ($\Delta G_v < 0$), when supersaturation occurs ($C > C_0$ and $s_s > 0$).

The reaction rate, k, can be expressed by a Born type equation (Eq. (2.17)), and it is directly related to the dielectric constant, ε. In this equation, ω is a constant determined by the reaction system, k_0 is reaction rate correspondent to the dielectric constant ε_0, R is the ideal gas constant and T is the absolute temperature.

$$\ln k = k_0 - \frac{\omega}{RT}\left(\frac{1}{\varepsilon} - \frac{1}{\varepsilon_0}\right) \tag{2.17}$$

The dielectric factor $(1/\varepsilon - 1/\varepsilon_0)$ remains close to 0 in subcritical conditions, which means that it does not have significance in this conditions. However, for supercritical conditions, this factor becomes relevant and its contribution gets significant, increasing the reaction rate and making the reaction in supercritical medium quicker than in subcritical. [32]

The use of supercritical fluids allows the achievement of a product dry and clean in a one step process, making it possible the avoidance of purification stages and large particle agglomeration. [33]

To sum up, supercritical fluids have the properties of liquid and gases and small adjustment of temperature and/or pressure can change the properties of the medium. Also, due to the low dielectric constant and the low solubility of metal oxides, the supersaturation degree is high resulting in the possibility to create nanoparticles.
The next section introduces the solvothermal synthesis technique to produce this nanoparticles.

2.2.2.2 Solvothermal Synthesis

Based on the advantages describe in the section 2.2.2.1, the technique selected to produce $Ce_{1-x}Zr_xO_2$ was supercritical continuous solvothermal synthesis. Other reasons to chose this method were the fact that can function in moderate conditions, increases the chemical reaction, improves mass transfer and assists in the stability of the products. In this method, the metal precursors are in an aqueous solution that will be mixed with a solvent in supercritical conditions and send to a reactor. After the reactor, the solution is quenched, followed by a back pressure regulator, then the nanoparticles are obtained after a filter, as it can be seen in Figure 2.6. [26] Although, the method of production applied in this thesis is slightly different and it will be explained in the section 3.3.

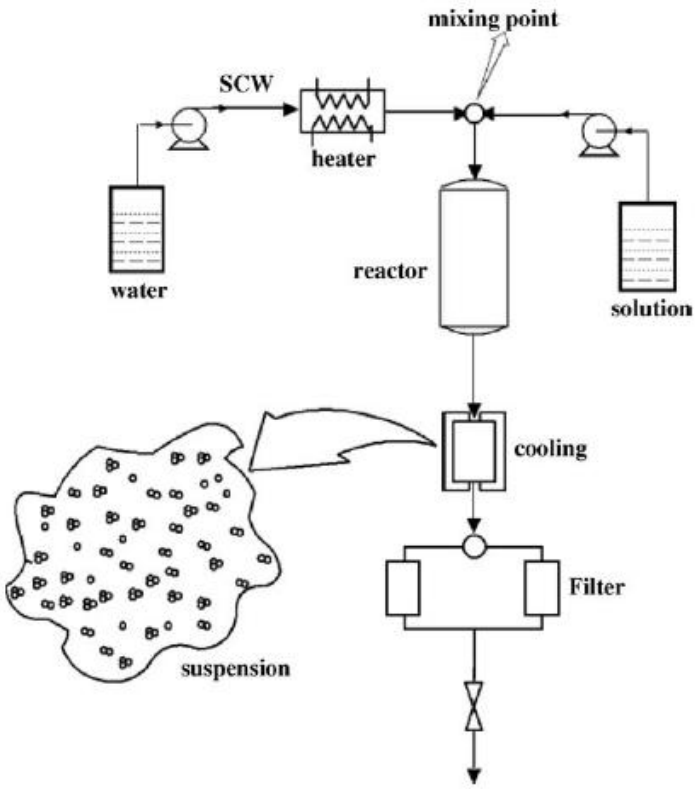

Figure 2.6: Apparatus for supercritical continuous hydrothermal synthesis. [26]

This method allows a short residence time, is easily controlled and the experimental conditions are reached almost right away. So, if there is a better control of reaction medium properties, consequently, there will be an improvement in the control of the materials characteristics. [23]

The reaction kinetics are accelerated by high temperatures, so it is important to guarantee that the solvent stays in the liquid form at this temperature. There are two ways to achieve this, using the non-hydrolytic route, resorting to solvents with high boiling points or controlling the pressure of the system, thus using the hydro/solvothermal route that leads to the application of supercritical fluids. [32]

If different solvents are applied, distinct particle sizes will be displayed due to different dielectric constants, that causes a difference in the solubility of the starting material. Also, by adjusting pressure and temperature of supercritical solvent, it is possible to obtain different surface morphologies and particle sizes. [20, 51, 21, 32]

In the case where water is the solvent, it is referred as supercritical continuous hydrothermal synthesis. For a metal (M) oxide this method has two parts: the Hydrolysis (Eq.(2.18)) and the Dehydration (Eq.(2.19)). So when a metal aqueous solution is heated up, metal hydroxides are formed due to shift of reaction equilibrium. At higher temperatures, the equilibrium shifts further towards the metal oxide formation. [52, 23, 37]

$$\mathrm{M^{x+} + xOH^- \longrightarrow M(OH)_x} \tag{2.18}$$

$$\mathrm{M(OH)_x \longrightarrow MO_{x/2} + {}^{x}/_{2}H_2O} \tag{2.19}$$

This technique permits the formation of nanoparticles because the supercritical conditions force the metal hydroxides to dehydrate rapidly before there is substantial growth. [53]

Also, the formation of nanoparticles using supercritical water (SCW) is because of the high hydrolysis reaction rate and the low solubility of the produced compounds in SCW. In this method, the reaction rate, equilibrium and solubility of metal oxides are controlled by the dielectric constant. [20, 30, 3]

Metal oxides have a higher solubility in subcritical water than in supercritical. However, in SCW the reaction occurs faster than in subcritical water because of the higher temperature and lower dielectric constant. So, when mixing metal aqueous solution with SCW, it is generated an extremely high degree of supersaturation and it happens rapid nucleation at the mixing point. Figure 2.7 represents the difference between the mechanism by sub- and supercritical conditions. For supercritical fluids, there is a rapid nucleation and the intermediate species are consumed in this step, obtaining this way smaller particles. [23]

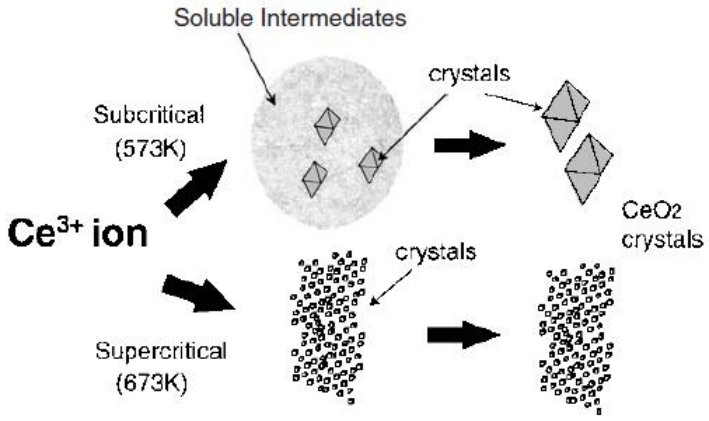

Figure 2.7: Mechanism of fine-particle production under supercritical conditions. [23]

For the case where alcohols are used as solvent, the dielectric constant (ε_r) decreases as the carbon chain grows, this also aids control the size of the particle. Also, as the polarity of the solution decreases, nucleation occurs earlier and the particles formed are larger. On the contrary, viscosity (mu) increases with the increasing chain growth. When the viscosity of the solution is high implies a low nucleation rate, which once again helps the growth process resulting in larger particle size.

It is important to note that due to the operative conditions in supercritical water ($\mathrm{T_c}$=374 ºC; $\mathrm{P_c}$=22,1 MPa) is necessary to use stainless steel with special characteristics to support the high temperatures and pressures simultaneously. [26]

Summing up, this technique allows a easy control of the characteristics of the particles produced, by changing factors such as residence time and solvent, etc, producing the catalyst support in a fast and one step way. The following section introduces other techniques to produce nanoparticles using supercritical fluids.

2.2.3 Other techniques using supercritical fluids

In this section, other methods to produce nanoparticles using SCF will be explained. All these methods have as basis the induction of a supersaturation state, which leads to the precipitation of particles, as it was for the case of solvothermal synthesis.

2.2.3.1 Rapid expansion of supercritical solutions

Rapid expansion of supercritical solutions is a technique where the supercritical solution which also contains a dissolved solute is expanded across a micro-orifice or nozzle. As consequence, the pressure will get lower and the solvent density will also decrease dramatically. The solute is this way rejected from solution and the SCF returns to the gas state.

The rapid pressure reduction leads to a very high supersaturation ratio, resulting in the precipitation of the particles. Smaller particles and narrower particle size distribution are achieved when the time for the solution to expand is smaller. The nozzle geometry also affects the particle size.

One of the disadvantages of this process is that the expansion is isenthalpic resulting in big temperature drops. As a way to overcome this problem, the nozzle is heated in order to avoid freezing. Other disadvantages are that the solute must be soluble in the SCF and that the particle size may be difficult to control. [52, 23, 25, 22]

2.2.3.2 Supercritical Anti-Solvent

An anti-solvent is a substance that when added to a solvent mixture promotes phase separation.

In this method, the solute is dissolved in a solvent. Then, the SCF is added as an anti-solvent, decreasing the solubility of the solution. Consequently, particles are formed with small diameter.

The phase separation that occurs when adding the anti-solvent is because of the changes in the physical properties of the solvent, such as the dielectric constant, the density and most importantly the chemical potential of the solute in the solution.

An advantage of this method is that the SCF can be easily recovered. Also, the solute just has to be soluble in the solvent and no in the supercritical fluid. A disadvantage is that an organic solvent is used, which means that it is necessary to consider the recycling and emissions of it and residual solvent in the particle. [23, 25, 22]

2.2.3.3 Particles from Gas-Saturated Solution

In this method, the material is melted and a SCF is dissolved in it. Then, the saturated solution is expanded across a nozzle, where it is cooled simultaneously by evaporation and Joule-Thompson effect. So, supersaturation conditions are reached, resulting in the escape of SCF formation of nanoparticles.

One of the advantages of this method is that the SCF reduces the melting point of the material, resulting in a lower temperature for the material to melt than normally. Another advantage is that the product is free of organic solvents.

Some disadvantages of this method are the relatively high operating temperatures and the problem of nozzle clogging. [23, 25, 22]

2.3 Characterization Techniques

This section introduces several techniques of characterization used to characterize the crystal structure, morphology, size, surface chemistry, etc.

The following section will describe the most relevant tools used to characterize the catalyst: Inductively Coupled Plasma - Atomic Emission Spectroscopy (ICP-AES), X-Ray Diffraction (XRD), Transmission Electron Microscopy (TEM), BET analysis and Oxygen Storage Capacity (OSC). Although the last one is not employed in this thesis.

2.3.1 Inductively coupled plasma - atomic emission spectroscopy

Inductively Coupled Plasma-Atomic Emission Spectrometry (ICP-AES) is an analytical technique used for elemental analysis. This technique is quick to realize and accurate, supporting a broad range of concentrations, from traces to high concentrations.

The sample must be in solution and normally it is dissolved in water. After this, the solution is transformed by a nebuliser into an aerosol. This creates big and small droplets ($1 - 10\mu m$), then they are separated in a spraychamber and the big ones go to waste, while the small ones go trough a plasma. The plasma is normally ionized argon which produces temperatures close to 7000℃, this temperature will cause the outer-shell electrons to excite.
These droplets transform in atoms and ions when they enter the plasma, in which first they are converted into salt particles by desolvation, then they split into individual molecules that fall apart in atoms and ions. As more energy is transferred into them, the excitation of their electrons to higher energy levels is promoted. Finally, when they return to their ground state, they emit electromagnetic radiation in the ultra-violet/visible range of the spectrum. This energy is unique and characteristic of each element depending in the electronic configuration of the orbital.
The qualitative and quantitative analysis can be made due to the fact that the energy transfer is inversely proportional to the wavelength of the electromagnetic radiation. The wavelengths emitted by the sample and their intensity are determined and the results are compared with reference standards being possible to determine the concentration. [54, 55, 56, 57]

Figure 2.8 represents a scheme of how a ICP-AES works.

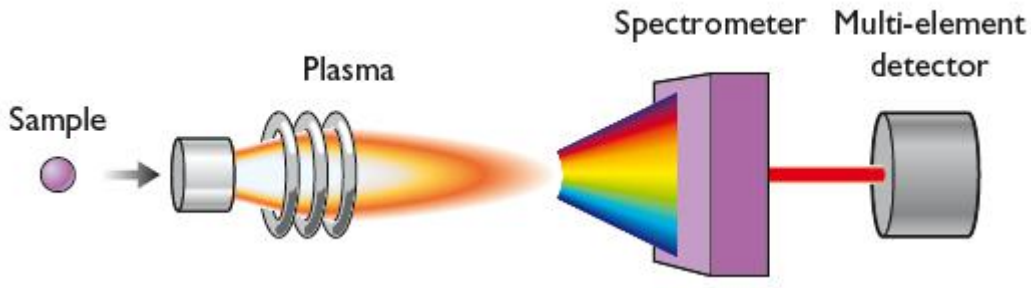

Figure 2.8: Operation of an ICP-AE. [54]

For this characterization technique, an amount of sample (around 5 mg) that is known is dissolved in a solution of 100 mL of acid and water (30% vol. of acid). The acid used was sulphuric acid (H_2SO_4).
The concentration of each individual component (cerium or zirconium) has to be between 0,5 mg/L and 100 mg/L in order to be possible to do the characterization.

2.3.2 X-Ray Diffraction

This technique is used to determine the crystal structure of the powder and can provide information on unit cell dimensions, as an example of the result of a XRD analysis (Figure 2.9). The X-ray pattern of each crystalline solid is unique and characteristic for each, allowing its identification. This technique is one of the most important characterization tool for solid state chemistry and materials science.

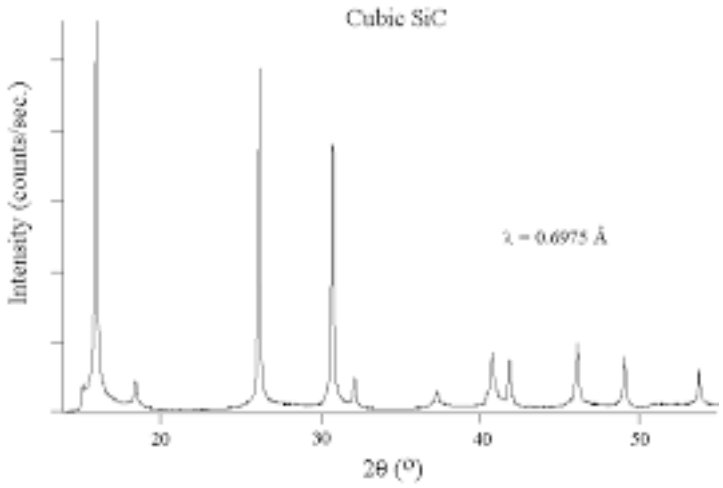

Figure 2.9: Example of experimental x-ray diffraction patterns of cubic SiC. [58]

For the XRD, the sample has to be in powder, so it's necessary to grind the sample to a fine powder and it has to be packed tightly, so that it gets strong intensities. A mortar is used to grind it and then the powder is put in a support of silicon substrate where it has to be well distributed. This support can be seen in Figure 2.10.

Figure 2.10: Support for XRD characterization.

In a more specific way, the X-rays are produced in a cathode ray tube by heating a filament to produce electrons, accelerating them towards a target by applying a voltage, and bombarding the sample with electrons. The characteristic X-ray spectra is produced when these electrons have sufficient energy to remove inner shell electrons of the sample. The X-rays are then aligned and directed to the sample. The intensity of the rays is recorded, as the sample and detector are rotated in a way that the sample is scanned through different 2θ angles, consequently all diffraction directions should be obtained due to the random orientation of the material. When the Bragg's Law ($n\lambda = 2d\sin\theta$) is satisfied, occurs a constructive interference and a peak of intensity happens. Finally, a detector records and process this signal and converts it to a count rate. The size and shape of the unit cell of the sample will affect the

directions of the diffractions, also the intensity of these depends of the kind and arrangement of atoms in the crystal structure. So, rays going through areas with high electron density will reflect strongly, oppositely the ones with low electron density will give weak intensities. [59, 60, 61]

In the diffractogram, the x axis is 2θ instead of θ because the geometry of the XRD equipment. More precisely, the X-ray is focused on the sample at an angle θ but the detector is mounted on an arm that collects the X-ray at an angle 2θ (Figure 2.11). The instrument that maintains the angle and rotates the sample is named goniometer (Figure 2.12). [60, 62]

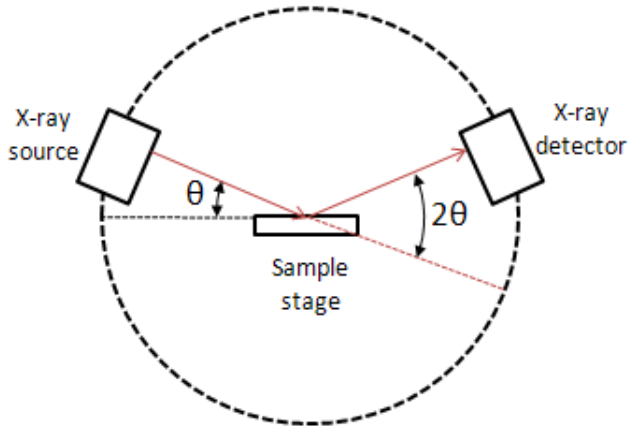

Figure 2.11: Explanation for 2θ axis. [62]

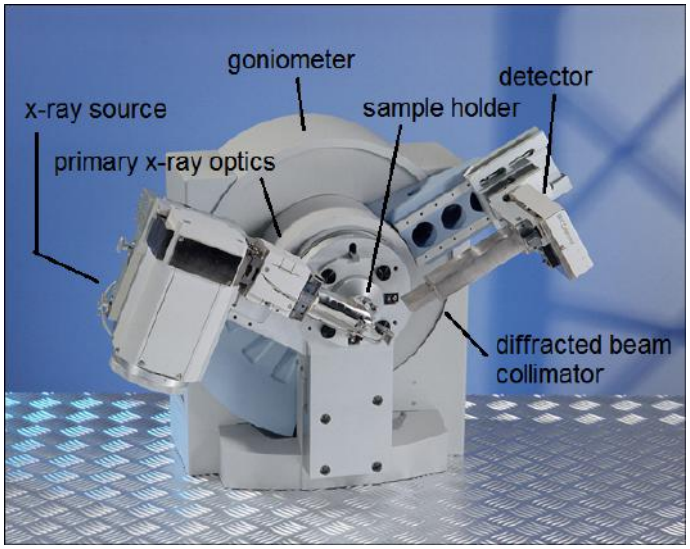

Figure 2.12: Illustration of a XRD equipment. [63]

This technique also allows to determine the crystallite size (d_{cr}) using the Scherrer Equation (Eq. (2.20)), where λ is the X-Ray wavelength (nm), θ is the position (°) and FWHM is Full Width at Half Maximum (°).

$$d_{cr} = \frac{0,89\lambda}{FWHM \times \cos(\theta)} \tag{2.20}$$

In addition, it is also possible to calculate the lattice parameter, resorting to Table 2.6 and Equations

(2.21) to (2.25).
The lattice parameter represents the physical dimension of unit cells in a crystal lattice. There are three lattice constants referred as a, b and c and there is also three angles that occur between them. In Figure 2.13, there is the representation of the lattice parameters.

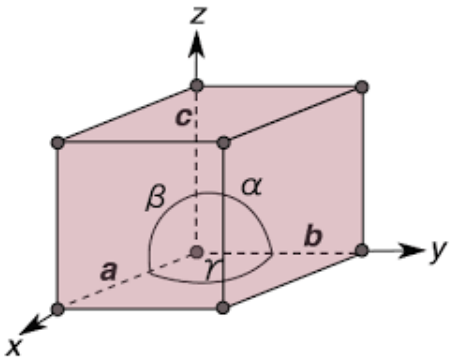

Figure 2.13: Representation of the lattice parameters.

Table 2.6: Conditions of the crystal systems.

Name	Conditions
Cubic	a=b=c; $\alpha = \beta = \gamma$= 90°
Hexagonal	$a = b \neq c$; $\alpha = \gamma$= 90°, β =120°
Monoclinic	$a \neq b \neq c$; $\alpha = \gamma$= 90°$\neq \beta$
Orthorhombic	$a \neq b \neq c$; $\alpha = \beta = \gamma$= 90°
Tetragonal	$a = b \neq c$; $\alpha = \beta = \gamma$= 90°
Triclinic	$a \neq b \neq c$; $\alpha \neq \beta \neq \gamma \neq$
Trigonal	a=b=c; $\alpha = \beta = \gamma$ ¡ 120°$\neq$ 90°

Table 2.7: Equations to calculate lattice parameter.

Crystal System	Equation	
Cubic	$\frac{1}{d^2} = \frac{h^2 + k^2 + l^2}{a^2}$	(2.21)
Hexagonal	$\frac{1}{d^2} = \frac{4}{3}\left(\frac{h^2 + hk + k^2}{a^2}\right) + \frac{l^2}{c^2}$	(2.22)
Monoclinic	$\frac{1}{d^2} = \frac{1}{\sin^2\beta}\left(\frac{h^2}{a^2} + \frac{k^2 sin^2\beta}{b^2} + \frac{l^2}{c^2} - \frac{2hl\cos\beta}{ac}\right)$	(2.23)
Orthorhombic	$\frac{1}{d^2} = \frac{h^2}{a^2} + \frac{k^2}{b^2} + \frac{l^2}{c^2}$	(2.24)
Tetragonal	$\frac{1}{d^2} = \frac{h^2 + k^2}{a^2} + \frac{l^2}{c^2}$	(2.25)

2.3.3 Transmission Electron Microscopy

In order to observe the morphology of the sample is used Transmission Electron Microscopy technique, which it is able to give precise information with a small volume of sample and distinguish the shape and the size of the particles. Besides this, TEM also allows to do chemical analysis.

The TEM equipment is composed by a cylindrical tube, which is in vacuum so that the molecules of gases do not absorb electrons. The electrons are formed in a cathode that emits them, then they are accelerated through an anode, finally going through an aperture into the vacuum tube.
Around the tube, there is electromagnetic lenses which are formed by coils and control the electron beam, that must be small, thin and coherent. This lenses direct the beam to the center of the tube where the sample is located. When the electrons pass the sample they will be affected by it, causing the electrons to continue down the tube with different energies. This will allow an image to be formed when they reach an image plane being here detected.
So, the areas which are darker mean that there was a greater absorption of electrons by the sample, while the lighter ones are the opposite, meaning the fewer or none electrons were absorbed. In a way, what is possible to see is the ”shadow” of the sample. In Figure 2.14 is possible to see a scheme of the TEM equipment. [64, 65, 66, 67]

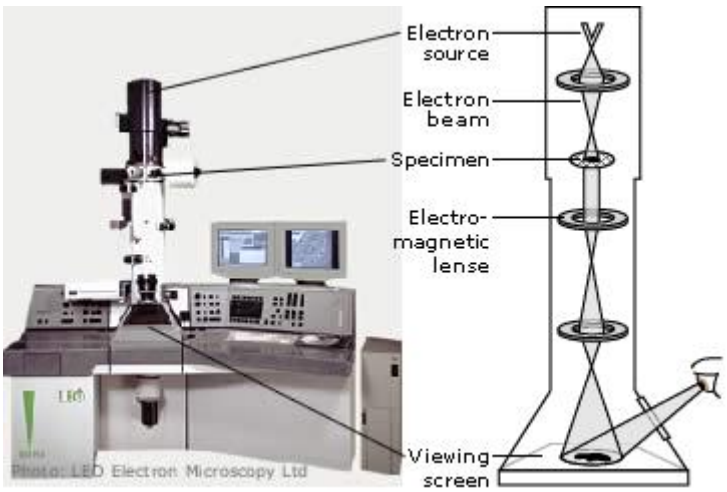

Figure 2.14: Illustration of a TEM equipment. [64]

For the characterization, a small amount of sample is dissolved in ethanol in a bottle of 3 mL, then the sample is subjected to an ultrasonic bath for 15 minutes to help the dissolution of the nanoparticles.
Finally, it is put in a TEM grid a drop of the solution and let to dry at room temperature. The grid support is observable in Figure 2.15.

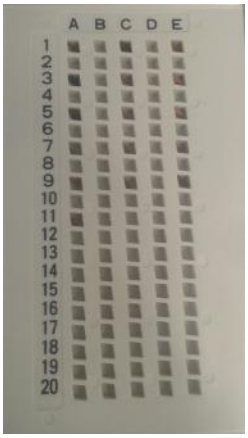

Figure 2.15: Grid for TEM characterization.

2.3.4 BET analysis

This method provides the specific surface area of a powder and also porous materials and this is determined by the physical adsorption of a gas on the solid surface, then calculating the amount of adsorbate gas corresponding to a monomolecular layer on the surface.
Normally, the gas used is nitrogen and the temperature for the procedure is that of liquid nitrogen. The result is the specific surface area in m^2/g.

So, this method works by obtaining an Adsorption Isotherm. This is possible by measuring the amount of gas adsorbed across a wide range of relative pressures at a constant temperature. Then, the BET (Brunauer, Emmett and Teller) equation (Eq. (2.26)) is applied. This equation is the most commonly used to describe the specific surface area.
In this equation, W is the weight of gas adsorbed, P/P_0 is the relative pressure, W_m is the weight of adsorbate as monolayer and B is the BET constant.

$$\frac{1}{W((P_0/P)-1)} = \frac{1}{W_m B} + \frac{B-1}{W_m B}\left(\frac{P}{P_0}\right) \tag{2.26}$$

By doing a linear plot of $1/[W(P/P_0)-1]$ against P/P_0 is possible to obtained the weight of adsorbate as monolayer (W_m). With this value and resorting to Equation (2.27) and (2.28), the value of the specific surface area can be calculated.
In this equations, S_{Total} is the total surface area, N is the Avogadro's Number, s is the adsorption cross section of the adsorbing species, M is the molecular weight of the adsorbate gas, S_{BET} is the specific surface area and m is the mass of the solid sample or adsorbent.

$$S_{Total} = \frac{W_m N s}{M} \tag{2.27}$$

$$S_{BET} = \frac{S_{Total}}{m} \tag{2.28}$$

In order to do this characterization, the sample must first be degassed. This is an important step, so that gases and vapours that may have become physically adsorbed onto the surface after manufacture and during treatment, handling and storage are removed. If this stage is not done, then the specific surface area may be reduced or miscalculated because an intermediate area of the surface is covered with molecules of the previously adsorbed gases or vapours.
The degassing is achieved by heating the sample under a vacuum under a flow of dry, inert gas. The temperature applied for degassing must not be too high in order to not affect the nature of the surface and the integrity of the sample. [68, 69, 70, 71]
For this case, the samples are degassed at 150 ℃ under vacuum during the night.

The equipment used for this analysis can be seen in Figure 2.16.

Figure 2.16: Illustration of a BET analysis equipment.

2.3.5 Oxygen Storage Capacity

Ceria is capable to accumulate oxygen when the phase is rich in O_2 and release it when the partial pressure of oxygen decreases, because of the quick balance between Ce^{4+} and Ce^{3+}. This capability is determined by measuring the oxygen storage capacity (OSC), which is defined as the maximum amount of oxygen that can be stored inside the catalyst.

OSC is measured using the same equipment as for the Temperature Programmed Reduction (TPR) analysis.
This method determines the number of reducible species present on the catalyst surface and reveals the temperature at which the reduction of each species occurs. The only characteristic that the sample must have to be able to do this analysis is to contain reducible metals.
The analysis occurs by flowing a gas (normally hydrogen in an inert carrier gas for instance nitrogen or argon) through the sample, usually at ambient temperature. Then with the gas flowing, the temperature of the sample is increased linearly with time and the consumption of hydrogen is monitored. In the downstream, the concentration of the gas mixture is measured and compared with the initial value, determining the volume of hydrogen uptake and consequently the average oxidation state of the solid after reduction. [72, 73, 74, 75]

In Figure 2.17, it can be seen an example of equipment which can be used to do the Temperature Programmed Reduction analysis.

Figure 2.17: Illustration of a TPR analysis equipment. [76]

Chapter 3

Methodology

This chapter consists of the description of the principal experimental conditions applied in this thesis, such as chemicals, temperatures, pressures and residence times used, and also equipment utilised.

3.1 Chemical Compounds

All the chemical compounds used were of the brand *Sigma-Aldrich*.
The precursors which were chosen for the synthesis of the $\mathrm{Ce_xZr_{1-x}O_2}$ catalyst support were Ammonium Cerium Nitrate ($\mathrm{Ce(NH_4)_2(NO_3)_6}$) with an assay of $\geq 98,5\%$ for cerium and Zirconium Oxynitrate Hydrate ($\mathrm{ZrO(NO_3)_2 \cdot xH_2O}$) with an assay of 99% for zirconium.
The precursors choice was made based on reference [32] where for cerium, this precursor got the best results in relation to size and surface area and for zirconium, it was shown that it worked well doping the cerium. For doping, it would have been better to use a precursor of ammonium nitrate for zirconium so as to reduce the influence of ligands in the characteristics of the powder, but it was not possible because it is unavailable.
The solvents used were propanol or 1-propanol ($\mathrm{C_3H_7OH}$) with an assay of $\geq 99,5\%$ and distilled water. For doping, distilled water was initially used as solvent to serve as a comparison base to the next phase of the project where different alcohols were tested.
Table 3.1 shows the relevant characteristics of the solvents used, where T_c and P_c are the critical temperature and pressure of the solvent, respectively and ρ_r and ρ_i are the densities in the reactor (experimental temperature and pressure) and in inlet (experimental pressure and 25℃), respectively.

Table 3.1: Characteristics of the solvents. [32]

	T_c (℃)	P_c (MPa)	ρ_r (kg/m^3) (T=300℃)	ρ_r (kg/m^3) (T=400℃)	ρ_i (kg/m^3)
Water	374	22,1	742,2	157,1	1007,8
Propanol	263,6	5,2	503	-	818,3

3.2 Operating parameters

The main operating parameters are pressure (P), temperature (T), flow rate (Q), concentration (C) and residence time (t_r).
The pressure applied in the system is 24,5 MPa and the temperature is 300℃ for when propanol is the solvent, when it is water the temperature was 400℃. The concentration chosen for the initial solution is 0,01 M. The residence time is also dependent of the solvent, for propanol, a residence time of 40 and 60 s was applied and for water 10, 30 and 60 s. In Table 3.2, there is a resume of the parameters implemented.

Table 3.2: Resume of parameters.

C (M)	P (MPa)	Solvent	T (℃)	t_r (s)
0,01	24,5	Propanol	300	40; 60
		Water	400	10; 30; 60

First, the synthesis of ceria in propanol was done with a residence time of 60s to test the set up and make sure it was appropriate. Then, the doping of ceria with zirconium was realized in water where residence time was of 30s and the values of x selected were 0, 0,25, 0,50, 0,75 and 1.
In order to do know how the different residence times and solvents effect the catalyst support produced, the composition $Ce_{0,5}Zr_{0,5}O_2$ was chosen to produce more catalyst support and compare with the results obtain previously. Furthermore, the synthesis of zirconia was realized in propanol with $t_r = 60s$. The parameters of synthesis mention are resumed in Table 3.3.

Table 3.3: Comparison tests.

x	Solvent	t_r (s)
0	Propanol	60
0,50	Water	10
	Water	60
	Propanol	40

The flow rate was determined employing Equation (3.1), where Q is flow rate (L/min), V_r is reactor volume (dm^3) and t_r is residence time (min).

$$Q = \frac{V_r \rho_r}{t_r \rho_i} \tag{3.1}$$

When the solvent is propanol is not possible to do experiments below a residence time of 40s because the pump used as a maximum flow rate of 10 mL/min and with t_r below this, the value of Q would be exceeded. Although, if the tube size was other, it was possible to use lower values of residence time.

3.3 Set-up

In section 2.2, the method described for the continuous synthesis consists in the precursor solution injection by one via and the solvent already in supercritical conditions by another via into a mixer. Thus, in this design the reaction conditions are achieved in the mixer which can contribute to early precipitation. In order to avoid this, *ICMCB* created a new way to carry out this synthesis. In this new method there is just one injection via, where the precursors and solvent are mixed previously in a beaker then introduced in the set-up, causing the supercritical conditions to be reached just in the reactor. Also, the reactor is brought to the operating conditions prior of the injection of the mixture intent to be synthesized.

So, instead of the set up shown in Figure 2.6, the one in Figure 3.1 was used, where there is just one injection via and the precursor solution is the mixture between the precursor and the solvent. In this figure is also possible to observe a scheme of where a modification on temperature and pressure occurs throughout the synthesis. In the figure P_r and T_r are the pressure and temperature in the reactor, respectively and P_{amb} and T_{amb} are room pressure and temperature, respectively.

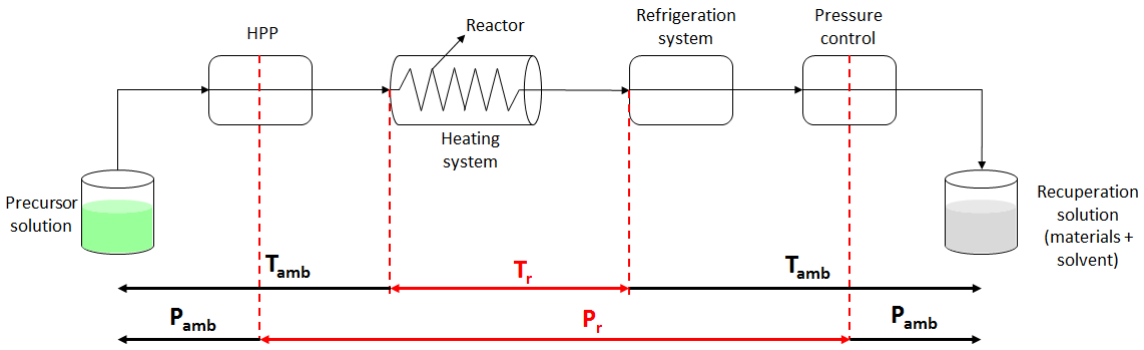

Figure 3.1: Scheme of temperature and pressure in the synthesis. [32]

In the Figure 3.2, there is a real image of the set up employed for the synthesis of ceria-zirconia in this thesis.

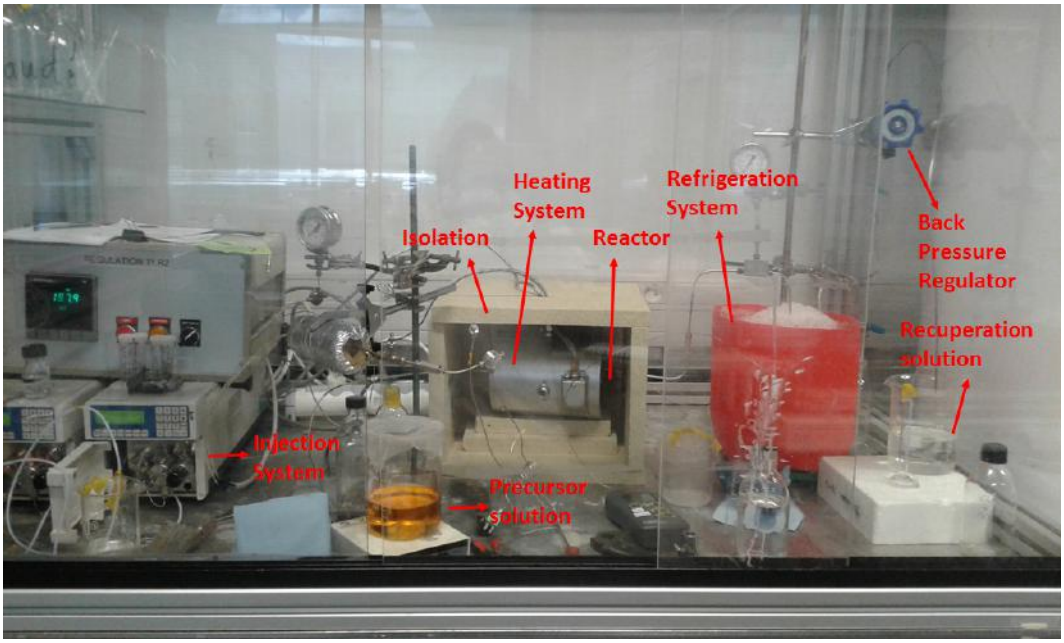

Figure 3.2: Apparatus used for supercritical continuous hydrothermal synthesis.

(a) Injection system.

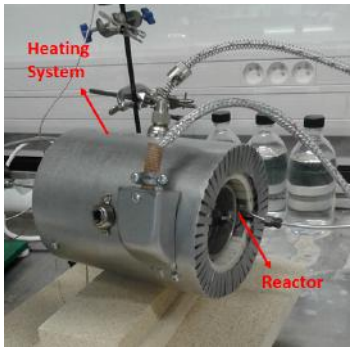

(b) Reactor.

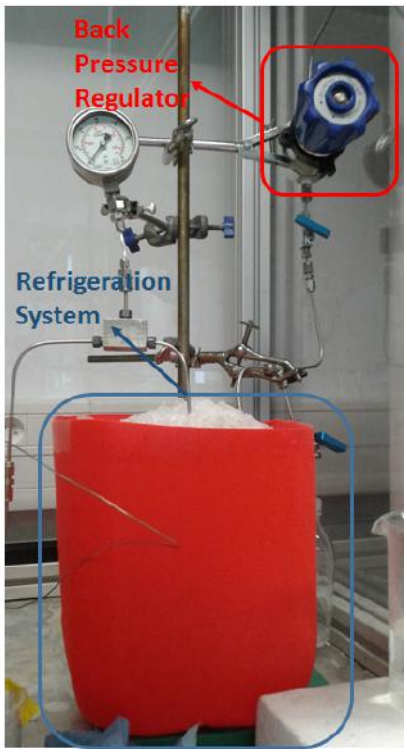

(c) Refrigeration system and Back pressure regulator.

Figure 3.3: Main components of set-up.

In this set-up, the main components are:

- **Injection:** composed by a high pressure pump (HPP) which injects the reaction mixture into the system through one channel (Figure 3.3a);
- **Reactor:** coiled tubular reactor with a length of 5 m installed in an insulated metal substrate. The temperature for the reaction is achieve using a ceramic heater and is controlled with a thermocouple in direct contact with the reactor, there is also another thermocouple in contact with the reactor outlet. To restrict heat losses, the reactor and heating system are enclosure in a thermally insulated material. The reactor is made from tube HP (high pressure) 1/8" ($D_{ext} = 3,19mm$ and $D_{int} = 1,57mm$) Stainless Steel 316 (Figure 3.3b);
- **Refrigeration system:** consists of a ice bath that is located after the reactor and before the back pressure regulator. Its function is to prevent the particles to grow more and keep them from aggregating (Figure 3.3c);
- **Back pressure regulator:** placed at the output of the system to control the pressure. It has two functions: maintain the pressure and to make the transition between the system and the ambient pressure (Figure 3.3c).

The solution obtained is a suspension of particles in the solvent. In order to recover them, it is necessary to filter the suspension. To do this, a centrifuge was used to extract most of the solvent and then a vacuum pump was used, finally the sample was let to dry long enough to ensure there is no solvent.

Chapter 4

Results and Discussion

This chapter will show all the results obtained from the characterizations done to the catalysts support produced ($Ce_{1-x}Zr_xO_2$) for different values of x, residence times and solvents. It is also included a discussion for this results and a section that compares the results obtained for the doping of ceria in water.

The sample names have the following configuration: Solvent-Percentage of Cerium-Temperature-Residence time. For the solvent, W represents distilled water and Pr 1-propanol. The unit for temperature is ℃ and for residence time is seconds (s).

When performing the synthesis of zirconia in propanol, no deposition or suspension of particles was noted, therefore it was not viable to realize characterizations on this sample. The reason for the lack of particles may be the fact that zirconium oxide is soluble in alcohols.

4.1 Effect of solvent in ceria synthesis

In a first instance, the effect of the solvent was studied in the synthesis of ceria. The solvents studied in this case was water and propanol.

So, initially, XRD was done in both samples, where the pattern results can be seen in Figure 4.1. This technique allowed the determination of the crystal structure, crystallite diameter and lattice parameter (a) of the samples. In Table 4.1, it is possible to check the crystallite size (d_{cr}) and the lattice parameter. The crystallite diameter was calculated applying Scherrer formula (Eq. (2.20)) on the profiles of the (111) peak.

Table 4.1: Crystallite size and lattice parameter (a) obtain with XRD pattern.

Sample	d_{cr} (nm)	a (Å)
Pr-100-300-60	4,8	5,408
W-100-400-30	6,7	5,413

The indexing values in Figure 4.1 were obtained from the database JPC with the program *EVA* for the code 03-065-5923.

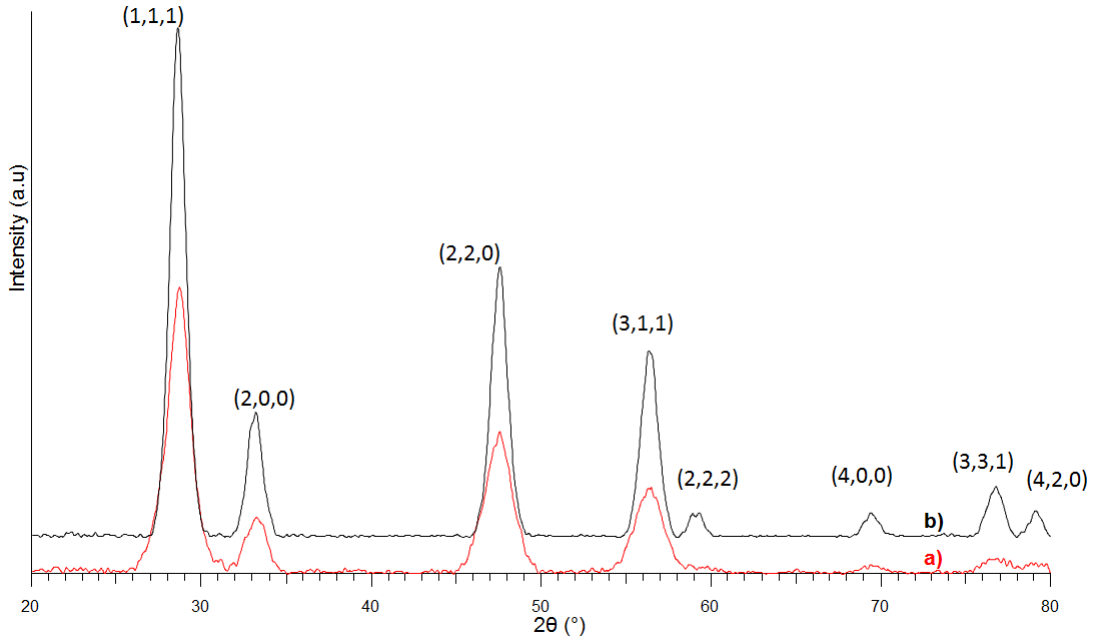

Figure 4.1: XRD patterns with the indexing values (h,k,l) of ceria. a) Pr-100-300-60, b) W-100-400-30

Comparing the values in Table 4.1, it is possible to see a difference between the crystallite sizes where the smaller one is achieve when the solvent is propanol.
Also, the XRD patterns allowed to confirm that the ceria prepared had the same crystal structure as pure ceria (cubic), due to the fact that the peaks correspond to the ones expected for this material. Furthermore, as Table 4.1 shows, the lattice parameter is very similar between both samples, indicating that the location of the peaks is similar and consequently, that the crystallite structure is the same.
The broad peaks seen in the diffraction patterns (Fig. 4.1) indicate that the samples are nanocrystals materials, supporting the results in Table 4.1 for crystallite diameter.

Next, TEM analysis was done. With this technique, it was possible to obtain an image of the sample produced and also determine the distribution size of the nanoparticles that compose the catalyst support, and therefore see the average size of them.

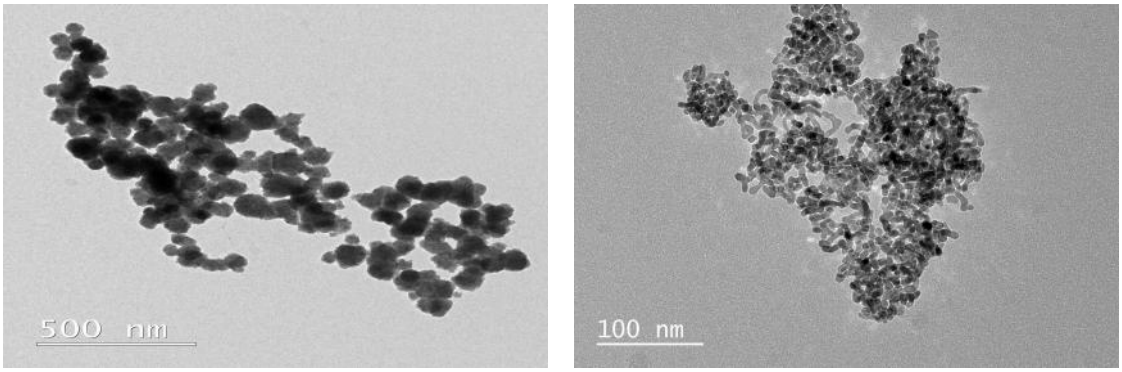

(a) Sample Pr-100-300-60 (b) Sample W-100-400-30

Figure 4.2: Images of pure ceria samples obtained via TEM.

With the images from Figure 4.2, it was possible to do distribution size analysis using the program *ImageJ*, where for the case when propanol is the solvent, 180 particles were sampled 180 particles and when it was water, 90 particles where studied to do the distribution size.

This distribution size analysis (Figure 4.3), it also allowed to calculate the average particle size that can be found in Table 4.2.
Another observation conceivable to do is that the nanoparticles produced with propanol as solvent have a sphere morphology, while the ones produced in water have a ”peanut” morphology. This last morphology is due to the sintering of two nanoparticles during the characterization, caused by the heat of the beam of the equipment being too strong and the particles too small, otherwise the particles would be spherical. So, for the samples realized in water, just the diameter of each nanoparticle was studied being this measurement considered the particle size.

The level of aggregation is also different depending on the solvent, for propanol bigger clusters are formed than for water. The particles aggregate to give a secondary structure in the form of spheres. This structures have a range of sizes between 30 and 120 nm in the case of propanol as solvent, where the nanoparticles size varies between 2 and 6 nm. For water as solvent, the agglomerates are smaller and the nanoparticles size varies between 3 and 8 nm.

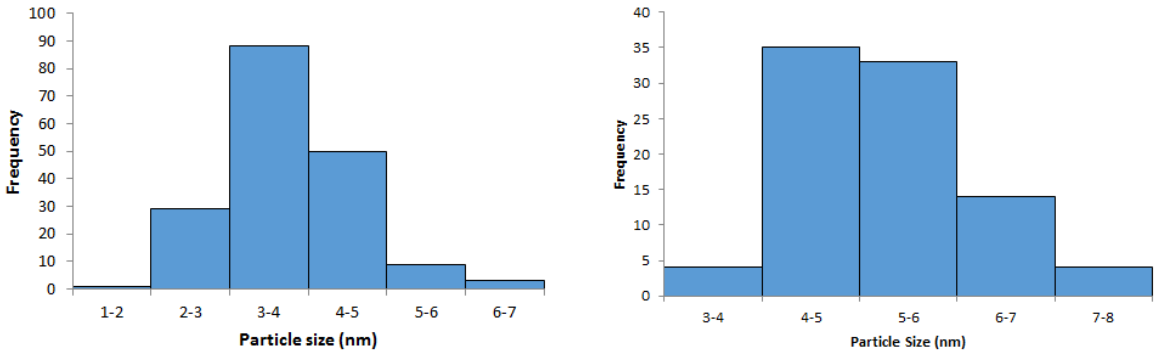

(a) Sample Pr-100-300-60

(b) Sample W-100-400-30

Figure 4.3: Distribution size of samples of ceria obtained via TEM analysis.

Table 4.2: Morphology and particle average size obtained via TEM analysis.

Sample	Morphology	Particle average size (nm)
Pr-100-300-60	Sphere	3,7±0,7
W-100-400-30	”Peanut”	5,2±0,7

From Table 4.2, it is possible to observe a decrease of the size as the solvent changes from propanol to water. This data goes according with the results obtained from the XRD patterns.

4.2 Effect of composition

In this section, the doping of ceria with zirconium was studied at a residence time of 30s at 400℃ with water as solvent. The percentages of cerium analysed were 100%, 75%, 50%, 25% and 0%.

Initially, in order to make sure that the doping has been done correctly and the quantity of cerium is the expected one, ICP analysis was realized. This analysis determines the quantity of cerium that effectively exists in the catalyst support after its production, this result is compared with the expected value of cerium in the precursor solution (Table 4.3).

Table 4.3: Comparison between initial and final % of cerium.

Sample	Theoretical % of cerium	Experimental % of cerium (ICP)
W-100-400-30	100	100
W-75-400-30	75	78
W-50-400-30	50	56
W-25-400-30	25	34
W-0-400-30	0	0

As it can be seen in Table 4.3, there is a slightly difference between the theoretical value and the real value. More specifically the quantity of cerium is always above of the expected meaning that not all the zirconium was integrated in the cerium. This may happen due to the difficulty that it was to dissolve the zirconium precursor in the solvent (distilled water). Perhaps, if microwave was used, it would have help the solubilization of everything.

After this initial characterization, the XRD patterns were obtained for the samples. Figure 4.4 represents the XRD patterns obtained for each sample and in Table 4.4 is possible to check the crystallite diameter and the lattice parameter.

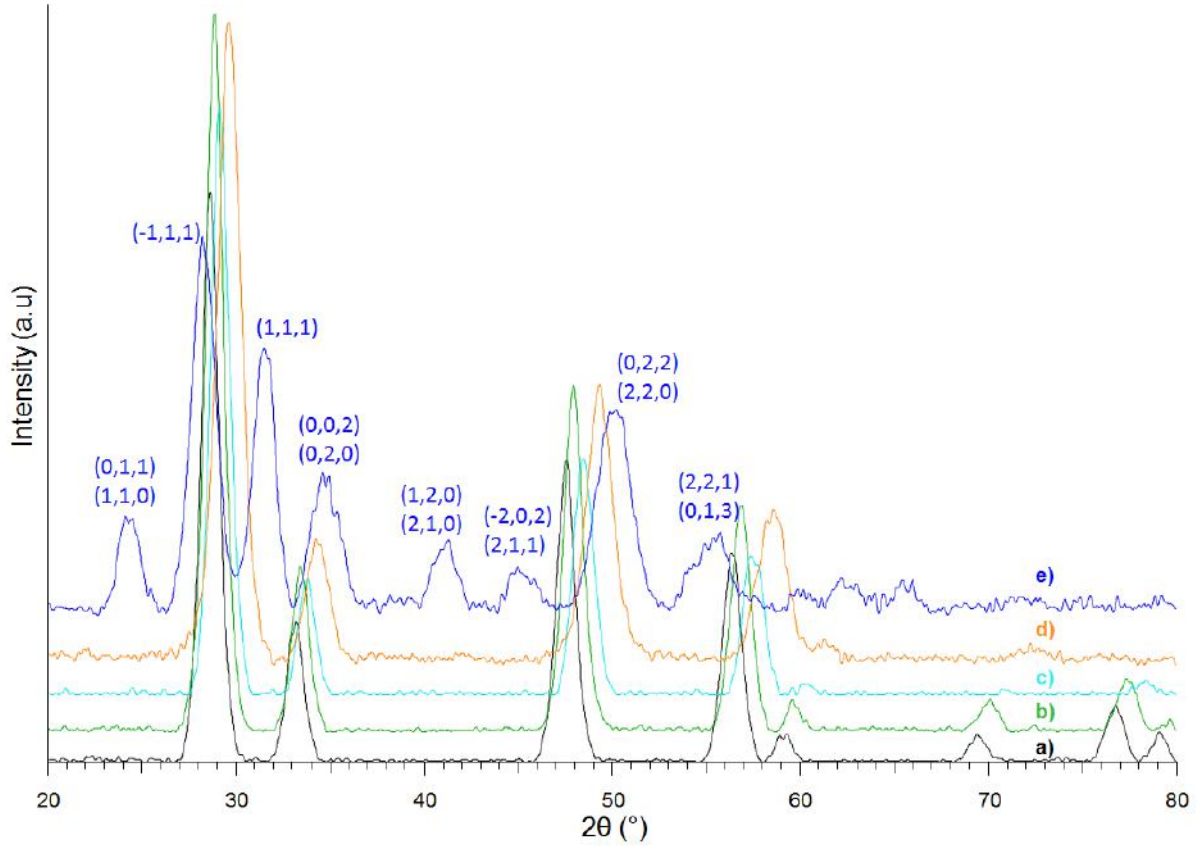

Figure 4.4: XRD patterns with the indexing values (h,k,l) of zirconia. a) W-100-400-30, b) W-75-400-30, c) W-50-400-30, d) W-25-400-30 and e) W-0-400-30

The indexing values in Figure 4.4 were obtained as before from the database JPC with the program *EVA* for the code 01-081-1314.

In order to better understand the evolution of the crystallite size and the lattice parameter, Figure 4.5 can be analysed where is clear that both this parameters increase with the increasing of cerium. It is

Table 4.4: Crystallite size and lattice parameter (a) obtain with XRD pattern.

Sample	d_{cr} (nm)	a (Å)
W-100-400-30	6,7	5,413
W-75-400-30	6,6	5,365
W-50-400-30	6,2	5,321
W-25-400-30	5,5	5,243
W-0-400-30	5,4	5,123

noteworthy that the values of percentage of cerium in the mentioned figure are the experimental. Also, in this figure there is a linear regression for the lattice parameter a and the corresponding coefficient of determination, where it is possible to see that the evolution of this parameter is almost linear with the increase of cerium in the sample.

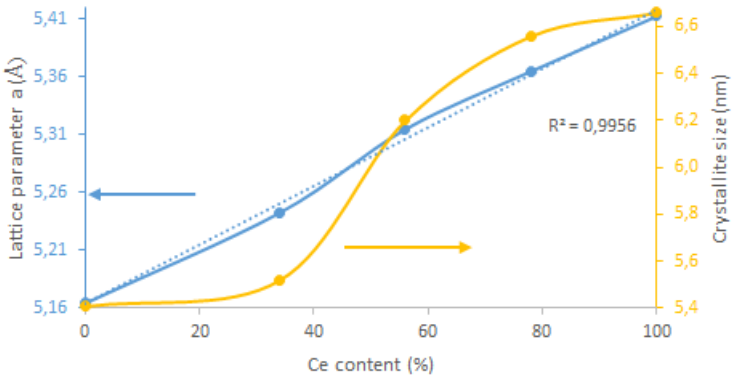

Figure 4.5: Lattice parameter and crystallite size evolution. In blue, there is the evolution of the lattice parameter a and in yellow the evolution of the crystallite size.

The XRD patterns allowed to confirm that ceria and ceria-zirconia mixed prepared had the same crystal structure as pure ceria (cubic) and that prepared zirconia had the same as pure zirconia (monoclinic). Also, the lattice parameter a for pure samples is similar to the ones expected, where for ceria was 5,41 and for zirconia was 5,17. For zirconia, the lattice parameters b and c were, as well, calculated which resulted in the values of 5,338 and 5,141, respectively.

As seen for pure ceria, the peaks from the diffraction patterns are broad indicating that the samples are nanocrystals materials, confirming the values for crystallite diameter present in Table 4.4.

From the XRD patterns (Fig. 4.4), it is possible to notice a shift in the characteristic peak of ceria around $2\theta = 28{,}542°$ to higher angle values as zirconium contents increases. This outcome is cause by the contraction of the lattice cell parameter when inserting Zr into CeO_2 fluorite lattice.
So, as it can be seen in Table 4.4, the crystallite diameter and the lattice parameter calculated decrease when the percentage of zirconium increases. This shrinkage of lattice cells indicates that the ions of Ce^{4+} with a ionic size of 0,097 nm are substituted by Zr^{4+}, which have a smaller ionic size (0,084 nm).

Next, TEM characterization was done in order to obtained an image of the samples and their particle size. Figure 4.6 shows the results of the TEM analysis.

Once more from Figure 4.6, the distribution size of the particles was studied for a sample of 90 particles. The result of this study can be seen in Figure 4.7 and in Table 4.5.

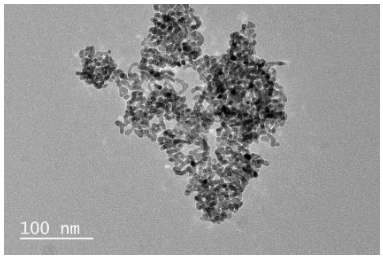

(a) Sample W-100-400-30

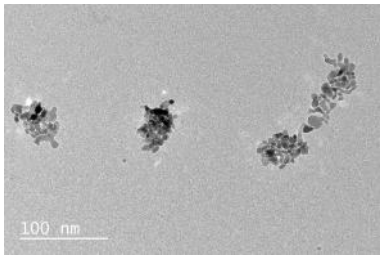

(b) Sample W-75-400-30

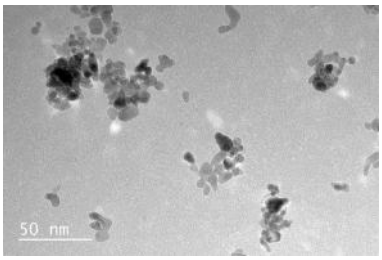

(c) Sample W-50-400-30

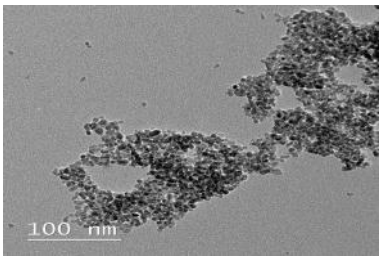

(d) Sample W-25-400-30

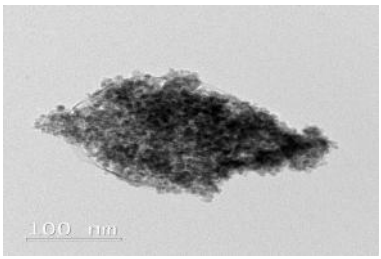

(e) Sample W-0-400-30

Figure 4.6: Images of samples obtained via TEM.

As it happened for the synthesis of ceria in water, the nanoparticles produced have a ”peanut” morphology and as explained before it is due to the sintering of the particles during the characterization. As it was performed for the case of ceria, it was just studied the diameter of each nanoparticle being this measurement considered the particle size.

Another observation conceivable to do is that the agglomerates are smaller, decreasing the cluster size when the percentage of cerium decreases. This may indicate that the agglomeration process can be linked with the pH of the synthesis medium, this happens due to the fact that the decomposition of the cerium ammonium nitrate yields to the formation of hydrogen ions (Equations (4.1)), reducing the pH value of the medium as the value of x decreases.

$$NH_4NO_3 + H_2O \longrightarrow NH_4^+ + NO_3^- + OH^- + H^+ \tag{4.1a}$$

$$NH_4^+ + OH^- \rightleftarrows NH_3 + H_2O \tag{4.1b}$$

The interstitial space between the nanoparticles in the agglomerates can act as pores, which in this conditions (supercritical conditions) are formed probably by the quick precipitation of the nanoparticles and consequently the coarse agglomeration because of the weak interaction between the oxide particles.

Table 4.5: Morphology and particle average size obtained via TEM analysis.

Sample	Morphology	Particle average size (nm)
W-100-400-30	”Peanut”	5,2±0,7
W-75-400-30	”Peanut”	4,9±1,3
W-50-400-30	”Peanut”	4,0±0,6
W-25-400-30	”Peanut”	5,0±0,9
W-0-400-30	”Peanut”	4,6±0,9

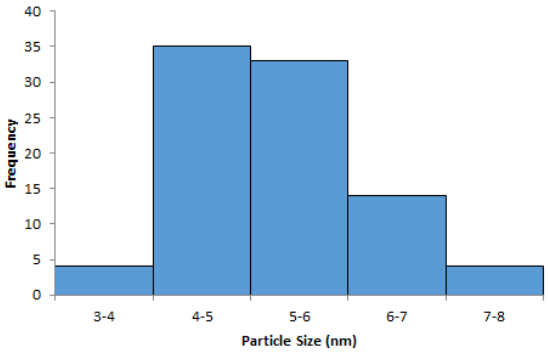

(a) Sample W-100-400-30

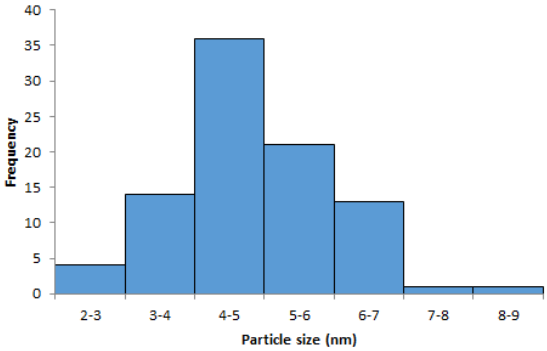

(b) Sample W-75-400-30

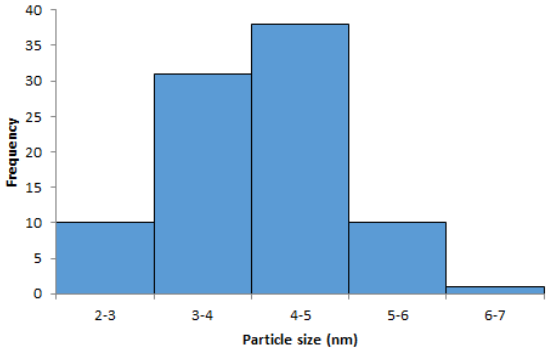

(c) Sample W-50-400-30

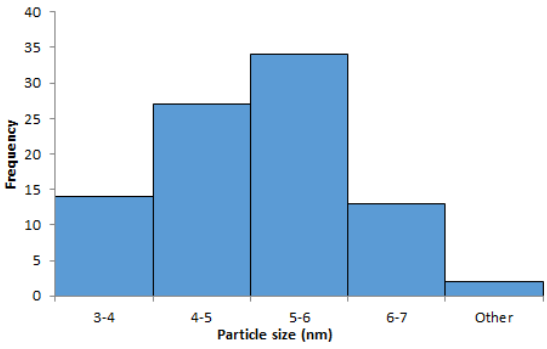

(d) W-25-400-30

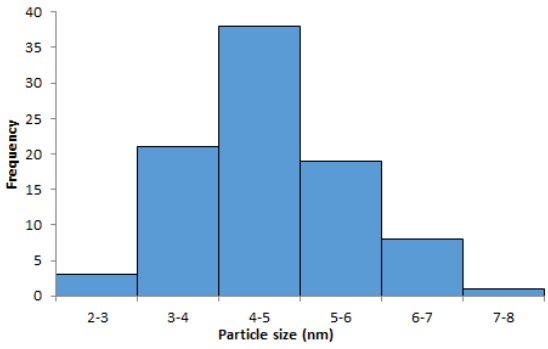

(e) W-0-400-30

Figure 4.7: Distribution size of samples obtained via TEM analysis.

From Table 4.5, it is possible to observe a decrease of the size with the increasing amount of zirconium although for the last two samples there is an increase and then decreases again. This small variation can be disregarded because of the small amount of particles studied and the fact that the analysis is done by hand increasing the error associated.

Following this characterization, the specific surface area was studied by doing a BET analysis and the results can be seen in Table 4.6.

As it can be seen the specific surface area is higher when the compounds are pure, especially in the case of ceria. Addressing the doped samples, it is clear that when the amount of zirconium increases the specific surface area also increases.
A high specific surface area is one of the most important characteristics for catalytic reactions due to the

Table 4.6: Determined specific surface area.

Sample	S_{BET} (m^2/g)
W-100-400-30	229
W-75-400-30	136
W-50-400-30	149
W-25-400-30	169
W-0-400-30	202

fact that they occur at the surface of the catalysts.

The increase of the specific surface area with zirconia in the doped samples can also be associated with the decrease of the density of the particles.

It is also important to point that just one test of BET analysis was done for each sample not guaranteeing that the behaviour would be the same if the analysis was repeated, thus justifying the values obtained.

4.2.1 Summary of the results obtain with water as solvent

In order to better compare the results of the doping of the ceria, a summary table (Table 4.7) was done which shows the most important values obtained.

Table 4.7: Summary table of results.

Sample	d_{cr} (nm)	Particle average size (nm)	S_{BET} (m^2/g)
W-100-400-30	6,7	5,2±0,7	229
W-75-400-30	6,6	4,9±1,3	136
W-50-400-30	6,2	4,0±0,6	149
W-25-400-30	5,5	5,0±0,9	169
W-0-400-30	5,4	4,6±0,9	202

Comparing the results, it is noticeable that the particles in the samples have a small size, and consequently they are able to achieve a high value of specific surface area. Also, the amount of zirconium in the sample has influence in this characteristics.

Another comparison able to be done is the small difference between the size obtain via XRD and TEM. This result indicates that the samples are monocrystals.

Finally, it is possible to see that the percentage of cerium does not have a big effect in neither the crystallite size nor the particle average size obtained via TEM because the difference between each percentage of cerium can almost be dismissed.

4.3 Effect of residence time in water

A brief study of the effect of the residence time was also done in the particles for a sample with 50% of cerium and using distilled water as solvent.
The resulting XRD patterns can be visualised in Figure 4.8, where is possible to see the similarity

between them in terms of intensity and position of the peaks, and also a disparity in the crystallite diameter, which can be analyse in Table 4.8.

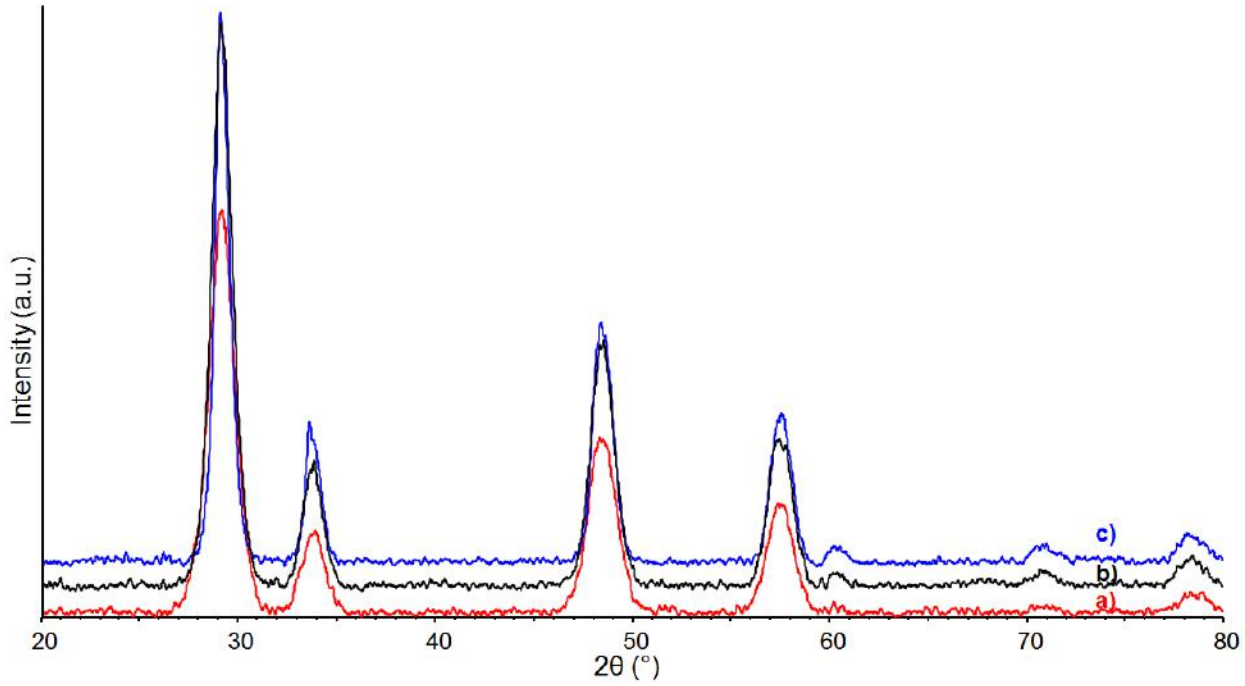

Figure 4.8: XRD patterns. a) W-50-400-10, b) W-50-400-30, c) W-50-400-60

Table 4.8: Effect of residence time and solvent on the crystallite size and lattice parameter.

Sample	d_{cr} (nm)	a (Å)
W-50-400-10	5,0	5,315
W-50-400-30	6,2	5,315
W-50-400-60	8,7	5,320

On Table 4.8, it can also be seen that the residence time has no effect on the lattice parameter as it was expected because the crystallite structure of the unit cell is the same for all the cases due to the fact that it has the same constitution.

In order to better understand the evolution of the crystallite diameter with the residence time, the graph in Figure 4.9 can be analysed. In there, an increase of the crystallite diameter with the increase of the residence time can be observed. This increment can be justified by the fact that because the particle stays more time in the reactor, it has the chance of growing for longer time, resulting in bigger particles.

4.4 Effect of solvent in ceria-zirconia oxide synthesis

In addition, as for the case of effect of the residence time, the effect of the solvent in ceria-zirconia oxide synthesis (50% cerium) was also studied. The solvent used was propanol.
For this solvent, a residence time of 30s was not applied, because of the capacity of the pump, as mentioned in Section 3.2, so a residence time of 40s was used due to being near enough for comparison be allowed and supported by the pump.

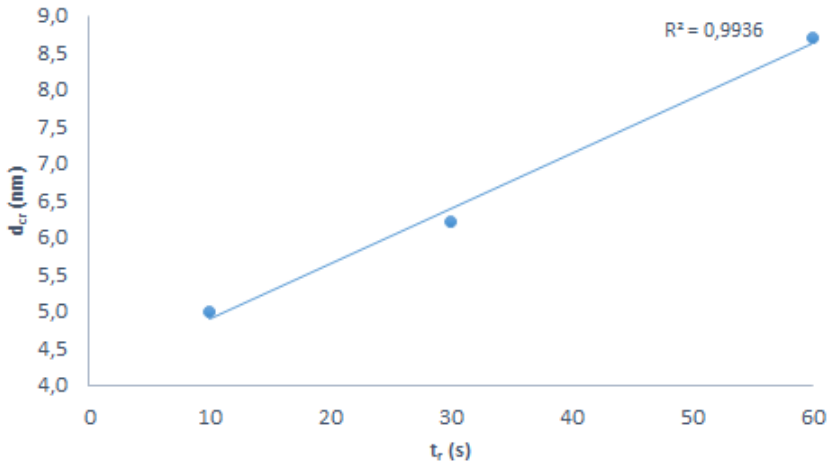

Figure 4.9: Evolution of crystallite size with the residence time.

The XRD pattern result can be seen in Figure 4.10 and the crystallite size and lattice parameter obtained from it can be consulted in Table 4.9.

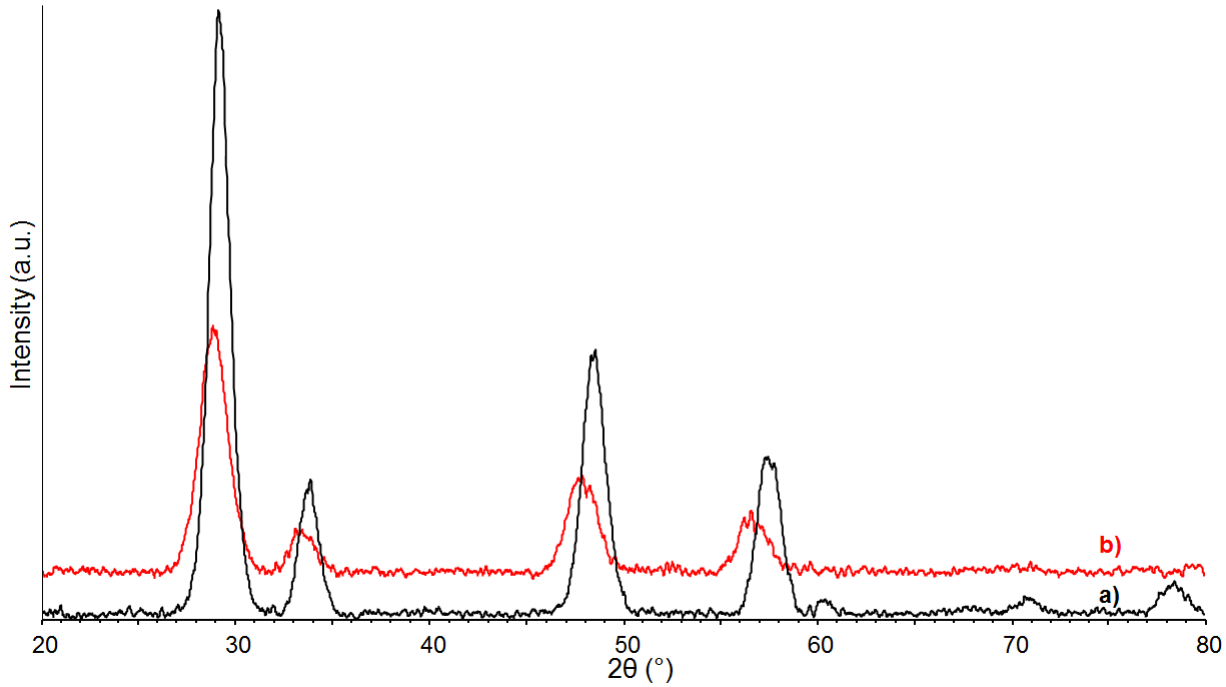

Figure 4.10: XRD patterns. a) W-50-400-30, b) Pr-50-300-40

Table 4.9: Effect of residence time and solvent on the crystallite size and lattice parameter.

Sample	d_{cr} (nm)	a (Å)
W-50-400-30	6,2	5,315
Pr-50-300-40	4,3	5,382

In Figure 4.10, it can be seen that there is a slightly shift of the peaks to the left when the solvent used is propanol. This has as consequence the fact that the values of lattice parameter do not match. This disparity may happen because the percentage of cerium when propanol is solvent, it is not the expected

due to the fact that as seen for pure zirconia the zirconium may be soluble in propanol, reducing its percentage in the sample, causing, consequently, the shift of the peak.

Also, as it was seen for pure ceria, the crystallite size is smaller for synthesis that have as medium propanol.

Chapter 5

Conclusion and Future work

5.1 Conclusion

In this thesis, the effect of solvent, composition and residence time in the synthesis of ceria and doped ceria with zirconium in supercritical conditions was studied.

For the effect of solvent in ceria, two different solvents were analysed, propanol and distilled water. This analyses was done for a residence time of 60s. It was noticeable that when the solvent is propanol the particles produced are smaller and it is also produced smaller clusters. For the case when the sample was doped with a ratio of 1 for a mixture of Ce/Zr and a residence time of 30s for distilled water and 40s for propanol, the crystallite size of the particles produced in propanol were once again smaller, not being done a further study to know about the clusters.

Next, for the study of the effect of composition, the synthesis was done in water for a residence time of 30s with compositions of 100%, 75%, 50%, 25% and 0% of cerium. First of all, it was possible to conclude that the percentage of cerium expected and the one obtained were slightly different, being the experimental bigger than the theoretical value, presumably because of the solubility of the zirconium precursor in water. Furthermore, the results allowed the conclusion that the quantity of cerium has little influence on the crystallite size and average size of the particle, although there is a small decrease with the decrease of cerium in the catalyst support. However, it was possible to see that the size of the clusters decrease with the increase of zirconium. In addition, it was observed that the crystallite size and the particle average size is similar indicating that the sample is composed of monocrystals.
In relation to the specific surface area, a disparity of values was noted ranging from 130 m^2/g to 230 m^2/g. It could not be determined a relation between the specific surface area and the quantity of cerium. Although, if the pure samples were dismissed, we can see an increase of the specific surface area with the decrease percentage of cerium. It is, also, noteworthy that just one analysis was made per sample so this values can be slightly different when repeated the analysis.

Finally, the effect of the residence time of a mixture of 50% of cerium ($Ce_{0,5}Zr_{0,5}O_2$) was studied in distilled water. The residence times analysed were 10s, 30s and 60s and it was observed that with the increase of the residence time, there was an increase of the crystallite size. This result was expected due to the fact that the more time the particle is inside of the reactor more it grows.

5.2 Future work

In order to complete this studied of doped ceria, the effect of different solvents in its synthesis will have to be examined, namely alcohols to see the consequence of the length of the carbon chain. Also, the effect of others precursors should be studied.
It is also important to determine the oxygen storage capacity of the samples in order to examine the maximum amount of oxygen that can be stored inside the catalyst and consequently help determine the best one for the methane reforming.
The BET analysis should be redone in order to confirm the results obtained.
Also, a optimization of the synthesis and characterizations should be studied regarding the lack of zirconium and its difficulty to solubilize. More specifically, the use of microwave should be tested.

Further work will include the study of the best way to do the modification of ceria-zirconia oxide with nickel nanoparticles and study the effect of the quantity of nickel in the catalyst properties. Also, it will be necessary to do a catalytic study in order to know how the catalyst produced behaves when applied in a reaction and how it deteriorates. This catalytic study will be performed in a dry methane reforming reaction.

Bibliography

[1] Joseph M. Desimone; William Tumas. *Green Chemistry Using Liquid and Supercritical Carbon Dioxide*. Oxford University Press, 2003.

[2] Isabel Arends Roger Arthur Sheldon and Ulf Hanefeld. *Green Chemistry and Catalysis*. Wiley-VCH, 2007.

[3] Tadafumi Adschiri, Youn-Woo Lee, Motonobu Goto, and Seiichi Takami. Green materials synthesis with supercritical water. *Green Chem.*, 13:1380–1390, 2011.

[4] Mike Lancaster. *Green Chemistry: An Introductory Text*. The Royal Society of Chemistry, 2002.

[5] Wen-Sheng Dong, Hyun-Seog Roh, Ki-Won Jun, Sang-Eon Park, and Young-Sam Oh. Methane reforming over ni/ce-zro2 catalysts: effect of nickel content. *Applied Catalysis A: General*, 226(1–2), 2002.

[6] Um-E-Salma Amjad, Antonio Vita, Camilla Galletti, Lidia Pino, and Stefania Specchia. Comparative study on steam and oxidative steam reforming of methane with noble metal catalysts. *Industrial & Engineering Chemistry Research*, 52(44), 2013.

[7] P.P.C. Udani, P.V.D.S. Gunawardana, Hyun Chan Lee, and Dong Hyun Kim. Steam reforming and oxidative steam reforming of methanol over cuo–ceo2 catalysts. *International Journal of Hydrogen Energy*, 34(18), 2009.

[8] Yun Hang Hu and Eli Ruckenstein. Catalytic conversion of methane to synthesis gas by partial oxidation and $\{CO2\}$ reforming. volume 48 of *Advances in Catalysis*, pages 297 – 345. Academic Press, 2004.

[9] Hyun-Seog Roh, Ki-Won Jun, Wen-Sheng Dong, Sang-Eon Park, and Young-Soon Baek. Highly stable ni catalyst supported on ce–zro2 for oxy-steam reforming of methane. *Catalysis Letters*, 74(1):31–36, 2001.

[10] Sandra C. Dantas, Janaína C. Escritori, Ricardo R. Soares, and Carla E. Hori. Effect of different promoters on ni/cezro2 catalyst for autothermal reforming and partial oxidation of methane. *Chemical Engineering Journal*, 156(2):380 – 387, 2010.

[11] John N. Armor. The multiple roles for catalysis in the production of $\{H2\}$. *Applied Catalysis A: General*, 176(2):159 – 176, 1999.

[12] Prakash Biswas and Deepak Kunzru. Steam reforming of ethanol for production of hydrogen over ni/ceo–zro catalyst: Effect of support and metal loading. *International Journal of Hydrogen Energy*, 32(8):969 – 980, 2007.

[13] Prakash Biswas and Deepak Kunzru. Oxidative steam reforming of ethanol over ni/ceo2-zro2 catalyst. *Chemical Engineering Journal*, 136(1):41 – 49, 2008.

[14] N. Laosiripojana and S. Assabumrungrat. Methane steam reforming over ni/ce–zro2 catalyst: Influences of ce–zro2 support on reactivity, resistance toward carbon formation, and intrinsic reaction kinetics. *Applied Catalysis A: General*, 290(1–2):200 – 211, 2005.

[15] Erdogan Gulari and J. Chris Brown. Catalytic production of hydrogen gas by methanol reforming. *Fuel Chemistry Division Preprints*, 47(2):727 – 728, 2002.

[16] R. Pérez-Hernández, A. Gutiérrez-Martínez, J. Palacios, M. Vega-Hernández, and V. Rodríguez-Lugo. Hydrogen production by oxidative steam reforming of methanol over ni/ceo2ezro2 catalysts. *International Journal of Hydrogen Energy*, 36:6601 – 6608, 2011.

[17] S. Ted Oyama, Pelin Hacarlioglu, Yunfeng Gu, and Doohwan Lee. Dry reforming of methane has no future for hydrogen production: Comparison with steam reforming at high pressure in standard and membrane reactors. *International Journal of Hydrogen Energy*, 37(13):10444 – 10450, 2012.

[18] María Martha Barroso-Quiroga and Adolfo Eduardo Castro-Luna. Catalytic activity and effect of modifiers on ni-based catalysts for the dry reforming of methane. *International Journal of Hydrogen Energy*, 35(11):6052 – 6056, 2010.

[19] Prashant Kumar, Yanping Sun, and Raphael O. Idem. Comparative study of ni-based mixed oxide catalyst for carbon dioxide reforming of methane. *Energy & Fuels*, 22(6):3575–3582, 2008.

[20] Alessandro Trovarelli; Paolo Fornasiero. *Catalysis by Ceria and Related Materials*. Catalytic Science Series. Imperial College Press, second edition, 2013.

[21] Can Erkey. *Supercritical Fluids and Organometallic Compounds: From Recovery of Trace Metals to Synthesis of Nanostructured Materials.*, volume 1 of *Supercritical Fluid Science and Technology*. Elsevier, first edition, 2011.

[22] Philip G. Jessop; Walter Leitner. *Chemical Synthesis Using Supercritical Fluids*. Wiley-VCH, 1999.

[23] Ya-Ping Sun. *Supercritical Fluid Technology In Materials Science And Engineering*. Marcel Dekker, Inc., first edition, 2002.

[24] Tony Clifford. *Fundamentals of Supercritical Fluids*. Oxford University Press, 1999.

[25] Richard Smith; Hiroshi Inomata; Cor Peters. *Introduction to Supercritical Fluids: A Spreadsheet-based Approach*, volume 4 of *Supercritical Fluid Science and Technology*. Elsevier, 2013.

[26] E. Reverchon and R. Adami. Nanomaterials and supercritical fluids. *The Journal of Supercritical Fluids*, 37(1):1 – 22, 2006.

[27] What is a supercritical fluid? `http://sfe.kkft.bme.hu/en/current-research.html`. Accessed: 18-11-2016.

[28] M. K. Devaraju, Xiangwen Liu, Kikuchi Yusuke, S. Yin, and T. Sato. Solvothermal synthesis and characterization of ceria–zirconia mixed oxides for catalytic applications. *Nanotechnology*, 20(40):405606, 2009.

[29] Jeong-Rang Kim, Wan-Jae Myeong, and Son-Ki Ihm. Characteristics in oxygen storage capacity of ceria–zirconia mixed oxides prepared by continuous hydrothermal synthesis in supercritical water. *Applied Catalysis B: Environmental*, 71(1–2):57 – 63, 2007.

[30] Tadafumi Adschiri, Yukiya Hakuta, and Kunio Arai. Hydrothermal synthesis of metal oxide fine particles at supercritical conditions. *Industrial & Engineering Chemistry Research*, 39(12):4901–4907, 2000.

[31] Onursal Yakaboylu, John Harinck, K.G. Gerton Smit, and Wiebren de Jong. Supercritical water gasification of manure: A thermodynamic equilibrium modeling approach. *Biomass and Bioenergy*, 59:253 – 263, 2013.

[32] Cédric Slostowski. *Synthèse solvothermale supercritique de nanostructures d'oxyde de cérium*. PhD thesis, University of Bordeaux 1, 2012.

[33] J. Sierra-Pallares, E. Alonso, I. Montequi, and M.J. Cocero. Particle diameter prediction in supercritical nanoparticle synthesis using three-dimensional {CFD} simulations. validation for anatase titanium dioxide production. *Chemical Engineering Science*, 64(13):3051 – 3059, 2009.

[34] Dushyant Shekhawat; James J. Spivey; David A. Berry. *Fuel Cells: Technologies For Fuel Processing*. Elsevier, 2011.

[35] P. van Beurden. On the catalytic aspects of steam-methane reforming: A literature survey, 2004.

[36] Tianli Zhu and Maria Flytzani-Stephanopoulos. Catalytic partial oxidation of methane to synthesis gas over ni–ceo2. *Applied Catalysis A: General*, 208(1–2):403 – 417, 2001.

[37] Jeong-Rang Kim, Ki-Yong Lee, Myung-Ji Suh, and Son-Ki Ihm. Ceria–zirconia mixed oxide prepared by continuous hydrothermal synthesis in supercritical water as catalyst support. *Catalysis Today*, 185(1):25 – 34, 2012.

[38] Zhenyu Sun, Hongye Zhang, Guimin An, Guanying Yang, and Zhimin Liu. Supercritical co2-facilitating large-scale synthesis of ceo2 nanowires and their application for solvent-free selective hydrogenation of nitroarenes. *J. Mater. Chem.*, 20(10):1947–1952, 2010.

[39] Albertina Cabanas, Jawwad A. Darr, Edward Lester, and Martyn Poliakoff. Continuous hydrothermal synthesis of inorganic materials in a near-critical water flow reactor; the one-step synthesis of nano-particulate cezro ([space]=[space]0-1) solid solutions. *J. Mater. Chem.*, 11(2):561–568, 2001.

[40] Hyun-Seog Roh, Ki-Won Jun, Wen-Sheng Dong, Jong-San Chang, Sang-Eon Park, and Yung-Il Joe. Highly active and stable ni/ce–zro2 catalyst for {H2} production from methane. *Journal of Molecular Catalysis A: Chemical*, 181(1–2):137 – 142, 2002.

[41] Jeong-Rang Kim, Wan-Jae Myeong, and Son-Ki Ihm. Characteristics of ceo2–zro2 mixed oxide prepared by continuous hydrothermal synthesis in supercritical water as support of rh catalyst for catalytic reduction of {NO} by {CO}. *Journal of Catalysis*, 263(1):123 – 133, 2009.

[42] Pan Huang, Haoxi Jiang, and Minhua Zhang. Structures and oxygen storage capacities of ceo2-zro2-al2o3 ternary oxides prepared by a green route: supercritical anti-solvent precipitation. *Journal of Rare Earths*, 30(6):524 – 528, 2012.

[43] Toshiyuki Masui, Kazuyasu Fujiwara, Yumin Peng, Takao Sakata, Ken ichi Machida, Hirotaro Mori, and Gin ya Adachi. Characterization and catalytic properties of ceo2–zro2 ultrafine particles prepared by the microemulsion method. *Journal of Alloys and Compounds*, 269(1–2):116 – 122, 1998.

[44] Shigeyuki Somiya. *Handbook of Advanced Ceramics: Materials, Applications, Processing, and Properties*. Elsevier, second edition, 2013.

[45] M. Kempaiah Devaraju, Shu Yin, and Tsugio Sato. Morphology control of cerium oxide particles synthesized via a supercritical solvothermal method. *ACS Applied Materials & Interfaces*, 1(11):2694–2698, 2009.

[46] Y. Hakuta, S. Onai, H. Terayama, T. Adschiri, and K. Arai. Production of ultra-fine ceria particles by hydrothermal synthesis under supercritical conditions. *Journal of Materials Science Letters*, 17(14):1211–1213, 1998.

[47] Jixiang Chen, Qunying Wu, Jianxiang Zhang, and Jiyan Zhang. Effect of preparation methods on structure and performance of ni/ce0.75zr0.25o2 catalysts for ch4–co2 reforming. *Fuel*, 87(13–14):2901 – 2907, 2008.

[48] Tadafumi Adschiri, Yukiya Hakuta, and Kunio Arai. Hydrothermal synthesis of metal oxide fine particles at supercritical conditions. *Industrial & Engineering Chemistry Research*, 39(12):4901–4907, 2000.

[49] Govindhan Dhanaraj; Kullaiah Byrappa; Vishwanath Prasad; Michael Dudley. *Springer Handbook of Crystal Growth*. Springer, 2010.

[50] Supersaturation: Driving force for crystal nucleation and growth. `http://blog.autochem.mt.com/2011/03/supersaturation-driving-force-for-crystal-nucleation-growth/`. Accessed: 05-12-2016.

[51] Manoj Pudukudy and Zahira Yaakob. Catalytic aspects of ceria-zirconia solid solution: Part-i an update in the synthesis, properties and chemical reactions of ceria zirconia solid solution. *Der Pharma Chemica*, 6(1):188–216, 2014.

[52] Gerd Brunner. *Hydrothermal and Supercritical Water Processes*, volume 5 of *Supercritical Fluid Science and Technology*. Elsevier, 2014.

[53] Shin-Ichiro Kawasaki, Kiwamu Sue, Ryuto Ookawara, Yuichiro Wakashima, Akira Suzuki, Yukiya Hakuta, and Kunio Arai. Engineering study of continuous supercritical hydrothermal method using a t-shaped mixer: Experimental synthesis of nio nanoparticles and {CFD} simulation. *The Journal of Supercritical Fluids*, 54(1):96 – 102, 2010.

[54] Philips. *Inductively Coupled Plasma-Atomic Emission Spectrometry (ICP-AES)*, 2013.

[55] Icp-atomic emission spectroscopy (icp-aes). `http://www.rsic.iitb.ac.in/icp-aes.html`. Accessed: 23-08-2016.

[56] Icp-aes technique description. `http://minerals.cr.usgs.gov/gips/na/5process.html`. Accessed: 23-08-2016.

[57] Jonathan Melville. Inductively coupled plasma-atomic emission spectroscopy: Short report. Technical report, UC Berkeley College of Chemistry, 2014.

[58] Glenn A. Richard. Bragg's law and diffraction: How waves reveal the atomic structure of crystals. `http://www.eserc.stonybrook.edu/ProjectJava/Bragg/`. Accessed: 23-08-2016.

[59] Hanno zur Loye. X-ray diffraction: How it works, what it can and what it cannot tell us. Technical report, University of South Carolina, 2013.

[60] Barbara L Dutrow and Christine M. Clark. X-ray powder diffraction (xrd). `http://serc.carleton.edu/research_education/geochemsheets/techniques/XRD.html`. Accessed: 23-08-2016.

[61] X-ray diffraction (xrd). `https://xos.com/technologies/xrd/`. Accessed: 23-08-2016.

[62] Powder x-ray diffraction. http://chem.libretexts.org/Core/Analytical_Chemistry/Instrumental_Analysis/Diffraction/Powder_X-ray_Diffraction. Accessed: 04-12-2016.

[63] What is xrpd - x-ray powder diffraction? http://www.xrpd.eu/. Accessed: 04-12-2016.

[64] The transmission electron microscope. http://www.nobelprize.org/educational/physics/microscopes/tem/. Accessed: 23-08-2016.

[65] Brian J. Ford, Savile Bradbury, and David C. Joy. Transmission electron microscope (tem). https://global.britannica.com/technology/transmission-electron-microscope. Accessed: 23-08-2016.

[66] Transmission electron microscopy (tem). https://www2.warwick.ac.uk/fac/sci/physics/current/postgraduate/regs/mpags/ex5/techniques/structural/tem/. Accessed: 23-08-2016.

[67] Background information - what is transmission electron microscopy? http://www.ammrf.org.au/myscope/tem/background/. Accessed: 23-08-2016.

[68] John M. Zielinski and Lorna Kettle. Physical characterization: Surface area and porosity. Technical report, Intertek, apr 2013.

[69] Neal Leddy. Surface area and porosity. Technical report, Centre for Microscopy and Analysis, 2012.

[70] Brunauer-emmett-teller (bet) surface area analysis and barrett-joyner-halenda (bjh) pore size and volume analysis. http://www.lucideon.com/testing-characterization/techniques/brunauer-emmett-teller-surface-area-analysis-barrett-joyner-halenda-pore-size-and-volume-analys Accessed: 23-08-2016.

[71] Bet. http://particle.dk/methods-analytical-laboratory/surface-area-bet-2/. Accessed: 23-08-2016.

[72] Temperature-programmed reduction. https://vscht.cz/kat/download/lab_tpr_eng.pdf. Accessed: 23-08-2016.

[73] Technique temperature programmed reduction (tpr). http://www.micromeritics.com/Repository/Files/Autochem%20II%202920%20technique%20TPR.pdf. Accessed: 23-08-2016.

[74] M.A Reiche, M Maciejewski, and A Baiker. Characterization by temperature programmed reduction. *Catalysis Today*, 56(4):347 – 355, 2000.

[75] M. Fadoni and L. Lucarelli. *Temperature programmed desorption, reduction, oxidation and flow chemisorption for the characterization of heterogeneous catalysis. Theoretical aspects, instrumentation and applications*.

[76] Autochem ii 2920. http://www.micromeritics.com/Product-Showcase/AutoChem-II-2920.aspx. Accessed: 23-08-2016.